

A STUDY OF VACANCIES IN TUNGSTEN
QUENCHED IN SUPERFLUID HELIUM

Thesis for the Degree of Ph. D.
MICHIGAN STATE UNIVERSITY
RONALD JOSEPH GRIPSHOVER
1969

LIBRARY
Michigan State
University

This is to certify that the

thesis entitled

A Study of Vacancies in Tungsten
Quenched in Superfluid Helium.

presented by

Ronald Joseph Gripshover

has been accepted towards fulfillment
of the requirements for

Ph.D. degree in Physics

Jack Bass
Major professor

Date April 10, 1969

ABSTRACT

A STUDY OF VACANCIES IN TUNGSTEN QUENCHED IN SUPERFLUID HELIUM

By

Ronald Joseph Gripshover

A system has been constructed which permits the refractory body-centered-cubic metals to be annealed and quenched in the ultrapure conditions which exist in and directly above superfluid helium. Studies were made on vacancies quenched into fine tungsten wires and the subsequent annealing away of this quenched-in resistance. To determine the effective vacancy formation energy, E_f^V tungsten specimens are quenched from temperatures between 1500K and 3200K. The quenched-in resistance varies somewhat from specimen to specimen, but the effective formation energy obtained for the fast quench data is nearly the same for all specimens and equal to 3.1 ± 0.2 ev. This data, together with Schultz's data, establishes both the magnitude of the quenched-in resistance and the effective formation energy for fast quenched tungsten.

By studying how the quenched-in resistance varies with quench speed, it is shown that the equilibrium vacancy concentration is probably not being retained even with the fast quench speeds. By extrapolating the data to infinite quench speed we get an estimate of the equilibrium vacancy resistance. The extrapolation leads to an estimate of $E_f^V = 3.5 \pm 0.2$ ev. The extrapolated data is also used to test Flynn's theory of vacancy annealing during the quench. The theory fits the infinite quench speed data, but there is slightly too much scatter to state definitively that Flynn's theory is applicable. This theory yields a value of 1.4 ± 0.2 ev for the vacancy motion energy.

To study the annealing away of the quenched-in resistance, both isochronal and isothermal anneals were performed. There is a single major isochronal recovery stage in the range 800-1000K in quenched tungsten, consistent with Stage IV recovery in radiation damage and cold work studies. This single major recovery stage suggests that there is a single defect present, presumably the vacancy. The isothermal recovery curve has an "S" shape suggesting complex annealing processes. Isothermal anneals with change-of-slope measurements yield an effective motion energy of 1.5 ± 0.3 ev. This estimate of the effective motion energy is in good agreement with the estimate obtained from the Flynn theory analysis.

If we take our "best values" for the effective formation and motion energies, we obtain a value of about 5 ev ($3.5 \text{ ev} + 1.5 \text{ ev}$) for Q . This is in reasonable agreement with the 5.2 ev estimate of Danneberg. The maximum Q which would still be consistent with our data is $Q \sim 6$ ev. However, our data do not appear to be consistent with either $Q = 6.6$ ev, or with $E_m^V = 3.3$ ev obtained from recent radiation damage studies.

**A STUDY OF VACANCIES IN TUNGSTEN
QUENCHED IN SUPERFLUID HELIUM**

By

Ronald Joseph Gripshover

A THESIS

Submitted to
Michigan State University
in partial fulfillment of the requirements
for the degree of

DOCTOR OF PHILOSOPHY

Department of Physics

1969

657283

ACKNOWLEDGMENTS

I would like to thank my advisor, Dr. Jack Bass, for his invaluable guidance and assistance during the entire course of this work. I wish to thank Mr. John Zetts for assisting in taking much of the data and for many helpful discussions. I am indebted to Dr. J. M. Galligan for kindly supplying us with a very pure 2.0 mil tungsten specimen.

I would also like to acknowledge the financial support of the Atomic Energy Commission.

Finally, I wish to express my deepest appreciation to my wife, Sharon, whose support and encouragement throughout this work have been invaluable. I am also deeply indebted to her for performing much of the analysis and preparation of this manuscript.

TABLE OF CONTENTS

	Page
LIST OF TABLES.	v
LIST OF FIGURES.	vi
I. INTRODUCTION.	1
A. Imperfections in Metals.	1
B. Vacancy Formation Energy, E_f^v	1
C. Techniques for Measuring E_f^v	2
D. Vacancy Motion Energy, E_m^v	4
E. Techniques for Measuring E_m^v	5
F. Previous Work on Tungsten.	6
G. Previous Work on Molybdenum.	10
H. Present Experiment.	11
II. QUENCHING TECHNIQUE.	14
A. Specimen Preparation	14
B. Quenching Procedure.	16
1. Room Temperature Measurements	16
2. Lighting Procedure.	17
3. Temperature Determination.	19
4. Quenching under the Superfluid.	20
5. Determination of Quenched-in Resistance.	21
6. Advantages and Disadvantages.	21
III. APPARATUS.	23
A. Specimen Holder.	23
B. Cryostat.	25
C. Circuits.	27
1. DC Circuits	29
a. Measuring circuit	29
b. Heating circuit	31
c. Potential circuits.	34
2. AC Circuits	38
a. Constant current source	38
b. Amplifier	42
c. AC to DC converter	44
d. Readout devices	47
e. Calibration and evaluation	49

	Page
IV. TUNGSTEN QUENCHING RESULTS	51
A. Quench Speed Data	51
B. Fast Quench Tungsten Data	53
C. Dependence of Quenched-in Resistance on Quench Speed	58
D. Additional Tungsten Data	64
E. Experimental Accuracy of the Quench Data	67
F. Extrapolation	70
G. Flynn Theory Analysis	73
V. ANNEALING OF DEFECTS QUENCHED INTO TUNGSTEN.	77
A. Isochronal Anneals	78
B. Isothermal Anneals	85
1. Isothermal Anneal	85
2. Isothermal Anneal with Change-of- Slope Measurements	87
VI. MOLYBDENUM DATA	92
VII. SUMMARY	94
LIST OF REFERENCES	97
APPENDIX A Significance of the Superfluid	100
APPENDIX B Operational Amplifiers	102

LIST OF TABLES

Table		Page
1	Summary of Past Work on Tungsten.....	9
2	Summary of Past Work on Molybdenum.....	12

LIST OF FIGURES

Figure	Page
1. Isochronal Recovery of Irradiated Tungsten	8
2. Simplified Schematic of the capacitance Discharge Circuit . . .	18
3. Specimen Holder	24
4. Cryostat	26
5. Block Diagram of Circuits	28
6. Measuring Circuit	30
7. Heating Circuit	32
8. Quench Speed Control Capacitors	33
9. Capacitor Charging Circuit	35
10. Potential Circuits	36
11. Block Diagram of the AC Circuits	39
12. AC Constant Current Source	40
13. AC Amplifier	43
14. Twin T Network	45
15. AC to DC Converter	46
16. Diode Output to Resistive and Capacitive Loads	48
17. Quench Speed Graphs	52
18. Quench Speed versus Quench Temperature for Specimen C (1.2 mil)	54
19. Quench Speed versus Quench Temperature for Specimen A (1.0 mil)	55

Figure	Page
20. Fast Quench Data for Specimen A (1.0 mil)	56
21. Fast Quench Data for Specimens A, B, C, and D	59
22. Dependence of Quenched-in Resistance on Quench Speed for Specimen C60
23. Dependence of Quenched-in Resistance on Quench Speed for Specimen B62
24. Dependence of Quenched-in Resistance on Quench Speed for Specimen A63
25. Dependence of Quenched-in Resistance on Quench Speed for Specimen A with Constant Subtracted	65
26. Radiation Shield	69
27. Data Extrapolation for Specimen A	71
28. Extrapolated Infinite Quench Speed Data	72
29. $1/T_q$ versus $1/T_q$ Plots for the Flynn Analysis	75
30. Isochronal Anneals for Specimens Quenched from 2800K to 3000K	79
31. Isochronal Anneals for Specimens Quenched from Temperatures above 3200K	81
32. Second Order Analysis of the Data from Figure 31	84
33. Isothermal Anneal	86
34. Isothermal Anneal with Change-of-Slope Measurements	89
35. Isothermal Anneal with Change-of-Slope Measurements	90
36. Preliminary Molybdenum Data	93

I. INTRODUCTION

A. Imperfections in Metals

Many important properties of metals are affected by imperfections in the ideal lattice. A number of these properties are determined more by the nature of the imperfections than by the nature of the host crystal. Some well-known examples are: the electrical conductivity of semiconductors, the low temperature resistivity of metals, atomic diffusion, the mechanical and plastic properties of solids. To understand these properties, one must understand the nature and properties of the imperfections involved.

The simplest imperfection is a missing atom, or lattice vacancy. It is the imperfection which we wish to study. The study of the properties of the single vacancy standardly focuses upon two quantities, the vacancy formation energy E_f^V , and the vacancy motion energy E_m^V .

B. Vacancy Formation Energy, E_f^V

The fractional concentration of single vacancies $n_v(T)$ in a pure material in thermal equilibrium at a temperature T and zero pressure can be written in terms of the vacancy formation energy as $\frac{1}{}$

$$n_v(T) = \exp(-G_f^V(T)/kT) = \exp(S_f^V/k) \cdot \exp(-E_f^V/kT) \quad (1)$$

where T is the absolute temperature, k is Boltzman's constant, G_f^V is the Gibbs free energy per vacancy, and S_f^V is the entropy increase per vacancy. The pressure correction for metals at atmospheric pressure is negligible. If the equilibrium vacancy concentration could be measured

as a function of T , the slope of a plot of $\ln(n_v)$ versus $1/T$ would be $-E_f^v/k$. Typically, for pure metals, $E_f^v \sim 1$ electron volt (ev) and the fractional vacancy concentration at the melting point is less than 10^{-3} . Hence, to get an appreciable thermal equilibrium vacancy concentration, the metal must be at a high temperature.

C. Techniques for Measuring E_f^v

In theory the vacancy concentration can be studied by measuring any property of the material which is affected by the presence of vacancies, such as electrical resistance, specific heat, hardness, length, etc. The difficulty is that one must know to high accuracy how this property behaves in the absence of vacancies. This problem was solved by Simmons and Balluffi^{2/}. They showed that for a cubic crystal the vacancy concentration could be written as

$$n_v = 3 \left(\frac{\Delta L(T)}{L_{R.T.}} - \frac{\Delta a(T)}{a_{R.T.}} \right)^* \quad (2)$$

where $\Delta L(T)/L_{R.T.}$ is the fractional increase in the macroscopic length of the specimen from room temperature to T and $\Delta a(T)/a_{R.T.}$ is the fractional increase in the microscopic lattice parameter. By taking this difference, they showed that all effects not associated with the presence of vacancies are removed. While this is a direct method for determining the vacancy concentration, it has limited accuracy and it is not easily extended to high temperatures with presently available techniques. Also, since the vacancies are studied at thermal equilibrium, this method gives no direct information

*Strictly speaking, the left hand side of this equation is $n_v - n_i$, where n_i is the fractional interstitial concentration. At high temperatures in the metals of interest, n_i is almost surely much less than n_v , giving the above result.

about vacancy mobility. To date, this method has been most useful in establishing the vacancy concentration at the melting point and the validity of other techniques, such as quenching.

If a specimen is cooled sufficiently rapidly from a high temperature, most of the vacancies present before the quench are trapped in the material, allowing them to be studied at lower temperatures. Several methods can be used to study vacancies at these temperatures: 1) vacancy clusters can be viewed by electron microscopy; ^{3/} 2) individual vacancies, as well as clusters, can be seen and counted with a field-ion microscope; ^{4/} 3) length change between the quenched and unquenched specimen can be measured; 4) changes in the heat output can be observed at temperatures where the quenched-in resistance begins to anneal away; 5) resistivity increases can be measured, usually, though not always, at liquid helium temperatures. The last method is most commonly used because resistances can be accurately and precisely measured. Since it is used in this experiment, it will be described in some detail.

To find the vacancy concentration as a function of temperature with this method, the specimen is first carefully annealed to get a stable, vacancy-free, base resistance. This resistance is measured at liquid helium temperatures to keep the normal lattice resistance from masking the vacancy contribution to the resistance. The specimen is then quenched from a known temperature, and its resistance at helium temperature again measured. The vacancy concentration is assumed to be proportional to the increase in resistance. If equation (1) holds, a plot of the logarithm of the resistivity increase against the inverse quench temperature will yield a straight line whose slope is the formation energy divided by the Boltzmann constant.

In general, when quenching with a finite quench speed, one does not expect to retain all the vacancies originally present in thermal equilibrium at the quench temperature T_q . The data obtained will therefore not be expected to reproduce equation (1) exactly. When dealing with quench data analyzed in terms of equation (1) we will speak of an "effective formation energy", to distinguish the experimentally determined numbers from the "correct" formation energy.

The quenching technique has inherent in it several potential difficulties. It assumes that the increase in the base resistance is due solely to quenched-in vacancies, when, in fact, many things, such as changes in the internal structure of the specimen (grain boundaries, etc.), different impurity contributions, strains in the specimen, etc., could conceivably contribute to such a resistance increase. Each vacancy is also assumed to contribute the same amount to the resistivity increase. If there is vacancy-vacancy or vacancy-impurity clustering, this may not be true. Also it is assumed that all of the vacancies present at the quench temperature are quenched-in. This again may not be correct, especially when the specimen is quenched from very high temperatures. However if these difficulties are kept in mind, quenching experiments can be of great value. From them effective vacancy formation energies can be determined, and by measuring how the quenched-in resistance varies as a function of quench speed, one can obtain an estimate for the "correct" vacancy formation energy, as is described in Section IV of this thesis.

D. Vacancy Motion Energy, E_m^V

It is usually assumed that at constant temperature an excess vacancy concentration will anneal down to the thermal equilibrium concentration

according to the equation ^{5/}

$$\frac{dn_v}{dt} = -F(n_v) e^{-E_m^v/kT} \quad (3)$$

where E_m^v is the vacancy motion energy, and $F(n_v)$ is a function of the vacancy concentration whose form is determined by the details of the annealing process. If some function of n_v is measured, such as the vacancy resistivity ρ , it is assumed that

$$\frac{d\rho}{dt} = -F(\rho) e^{-E_m^v/kT} \quad (3a)$$

This assumption introduces some problems; first, ρ may not be proportional to n_v , and secondly, this equation assumes that the only mobile entity is the single vacancy. In a real experiment, small vacancy clusters, vacancy-impurity complexes, and other entities such as interstitials may also be mobile, and by their motion to sinks or to large clusters contribute to a change in resistivity. Therefore, when analyzing annealing data using equation (3a) we will speak of an "effective motion energy" to distinguish the experimentally determined quantity from the real motion energy of single, free vacancies. If $F(n_v)$ is proportional to n_v , the annealing process is said to be a "first order process" or to involve "first order kinetics". If $F(n_v)$ is proportional to $(n_v)^2$, the annealing process is said to involve "second order kinetics". We shall return to this equation in the analysis of the annealing data in Sections V and VI.

E. Techniques for Measuring E_m^v

E_m^v can be estimated most directly by studying the annealing of vacancies from a specimen. There are two annealing procedures generally used to

determine motion energies: isochronal annealing and isothermal annealing. An isochronal anneal consists in heating the specimen for a fixed time at each of a series of increasing temperatures until most of the quenched-in resistance anneals out. This gives the recovery as a function of the annealing temperature. An isothermal anneal consists in heating the specimen to a fixed temperature to obtain the recovery as a function of the annealing time. The detailed methods used for the calculation of E_m^V from annealing data will be discussed in conjunction with the analysis of the annealing data in Sections V and VI.

The quenching technique is the best method of producing vacancies in a metal at low temperatures without producing large concentrations of other defects. However, point defects (vacancies, interstitials, etc.) can also be produced by radiation damage and cold working. The difficulty with producing vacancies in these ways is that they represent only a fraction of the defects present, making it difficult to interpret the annealing data satisfactorily.

The vacancy motion energy can also be estimated if the vacancy formation energy E_f^V and the activation energy for self diffusion, Q , are known. If diffusion takes place by means of single vacancies, which appears to be the case for many pure metals, it can be shown that $E_m^V = Q - E_f^V$.^{6/}

F. Previous Work on Tungsten

There is only one short paper in the literature which reports quantitative quenching results on tungsten. In 1964 Schultz^{7/} published the results of quenching a single 1.2 mil tungsten wire using the superfluid technique. He obtained an effective vacancy formation energy of 3.3ev. By extrapolating

his data to the melting point and assuming that $n_v = 0.02 \frac{\Delta R_q}{R_{273}}$, where ΔR_q is the resistance that would be quenched-in during a quench from the melting point, he obtained a fractional vacancy concentration at the melting point of 1.1×10^{-4} .

Vacancies and other defects in tungsten have been investigated by several experimenters using techniques other than quenching. From measurements of the high temperature specific heat, Kraftmakher and ^{8/}Strelkov obtained a formation energy of 3.14eV and a vacancy concentration of 2.7 percent at 3600 degrees Kelvin (3600K). In this technique, the low temperature specific heat is linearly extrapolated to high temperatures and any deviation of the data from the extrapolation is considered to be due to vacancies. It is difficult to make this extrapolation accurately, and it is not likely that all deviations from linearity are due solely to vacancies. The formation energy they obtained is in reasonable agreement with that obtained by Schultz, but their vacancy concentrations are two orders of magnitude greater than Schultz's.

There have also been a number of radiation damage and cold work experiments with tungsten. On the next page is shown a typical isochronal ^{9/}recovery curve for radiation damaged tungsten. The fractional defect concentration is plotted as a function of the annealing temperature. The annealing stages have been labeled according to current practice. During each stage a particular defect becomes mobile and anneals away.

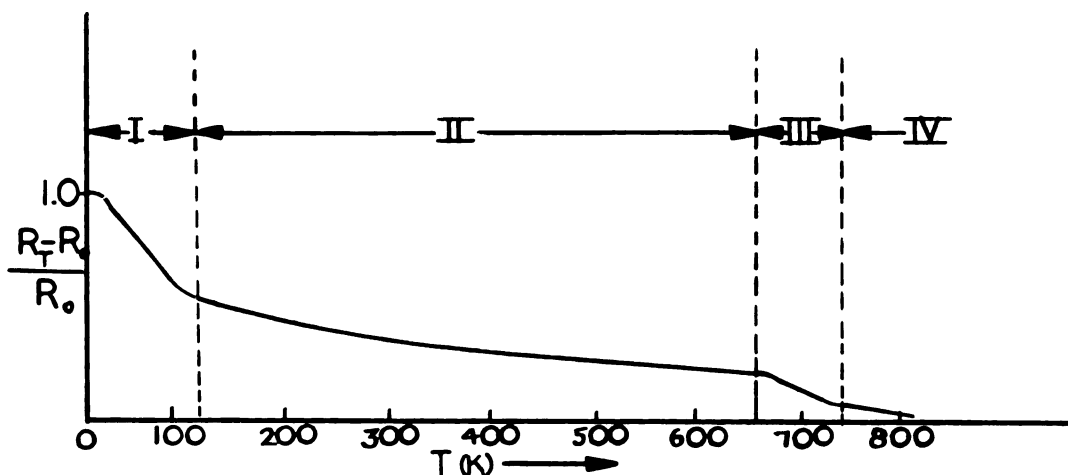


Figure 1: Isochronal Recovery of Irradiated Tungsten

Table 1 is a summary, in chronological order, of the previous work on tungsten. The remaining comments in this section will be in reference to this table. First note that there are no estimates for E_m^v , or for the temperature at which vacancies become mobile, obtained from annealing studies of quenched tungsten. Since vacancies are the predominant defect in quenched tungsten, one would expect that annealing studies of quenched tungsten would yield the most reliable values for both the temperature at which vacancies become mobile and E_m^v . Until the mid-sixties it was thought that vacancies became mobile in Stage III but recent work, especially the field ion microscopy work of Galligan, et. al., suggests that vacancies are not mobile until Stage IV. Consequently, the estimates for E_m^v have recently been increased from 1.7 ev to about 3 ev, and the estimate of the temperature at which vacancies become mobile has increased from the 600-700K range to the 700-1000K range.

The experimental values for Q listed in Table 1 are not mutually consistent. This rules out for the present any estimate of the vacancy motion

TABLE 1
SUMMARY OF PAST WORK ON TUNGSTEN

Investigator(s)	Method of Producing Vacancies	Temperature at which Vacancies Become Mobile (K)	E_m^V (ev)	E_f^V (ev)	Q (ev)	Ref.
V.P. Vasil'ev & S.G. Cherenko (56)					5.89	10
G.H. Kinchin & M.W. Thompson (58)	neutron irradiation	590	1.7			11
R.C. Koo (58)	cold work	620	1.7			12
H. Schultz (59)	cold work	Stage III, 570-670	1.73			13
R.H. Schnitzel (59)					5.42	14
M.W. Thompson (60)	neutron irradiation	Stage III, 620-720	1.7			9
L.A. Neimark & R.A. Swalin (60)	cold work	600-770	1.7			15
W. Danneberg (61)					5.2	16
Ya. A. Kraftmakher, P.G. Strelkov (63)	specific heat extrapolation			3.14		8
H. Schultz (64)	cold work					17
H. Schultz (64)	quenching			3.32		7
J. Moteff & J.B. Smith (65)	neutron irradiation	Stage IV, 1170				18
R.L. Andelin, J.D. Knight, M. Kahn (65)					6.6	19
M. Attardo & J.M. Galligan (66)	neutron irradiation	Stage IV, 720-970				4
D. Jeannotte & J.M. Galligan (67)	neutron irradiation	1140	3.3			20
L.K. Keys, J.P. Smith, J. Moteff (68)	neutron irradiation	Stage IV, 920-1270				21
C.P. Flynn (68)	----theoretical calculation----		2.8			22

energy from the relation, $E_m^V = Q - E_f^V$, until the value of Q is more firmly established for tungsten.

There have been only two theoretical papers published concerning the vacancy formation and motion energies for the body-centered cubic (bcc) transition metals. In 1963, Gregory published a short paper in which he used "reasonable" values for the quantities in equations (1) and (3) to conclude that "it may just be possible to quench in a measurable concentration of lattice vacancies in bcc transition metals."^{23/} In 1968, from an elastic theory of metals, Flynn calculated a vacancy motion energy of 2.8 ev for tungsten.

G. Previous Work on Molybdenum

No systematic study of vacancies quenched into molybdenum has been published. Meakin et. al.^{24/} quenched a molybdenum single crystal from vacuum into molten indium. They then used electron transmission microscopy to examine what they interpreted as vacancy loops. From the number of loops they saw, they estimate a fractional vacancy concentration at the melting point of 5×10^{-5} , from which they deduced a formation energy of 2.4 ev. Nihoul^{25/} performed "preliminary quenching experiments" by breaking the glass envelope of the specimen (immersed in water) when the specimen reached the desired temperature. He used the results of these experiments to strengthen his contention that vacancies do not become mobile until Stage IV in molybdenum. Kraftmakher, again using specific heat determinations,^{26/} obtained a formation energy of 2.24 ev and a vacancy concentration at the melting point of 4.3 percent. The formation energy obtained by Kraftmakher is consistent with Meakin's, but the vacancy concentration is higher by three orders of magnitude.

As with the tungsten, there have also been a number of radiation damage and cold work studies of molybdenum. These results, a recent calculation of E_m^V by Flynn, and measurements of Q for molybdenum, are summarized in Table 2.

H. Present Experiment

Vacancies in the common face-centered cubic (fcc) metals, especially gold, have been extensively studied.^{27,28/} Most of the above techniques have been applied to these metals. All of the quench techniques, as well as the Simmons-Balluffi technique, yield values for the vacancy formation energy which are mutually consistent. These studies serve to validate the quenching technique. The fcc metals were studied first because they are much easier to purify and to work with. They can be resistance heated in air and quenched by plunging them into water or some other suitable liquid, or by merely turning off the current and allowing them to cool in air.

This is not the case for bcc transition metals. Only recently have these metals been purified sufficiently for meaningful quenching experiments to be performed on them. They also contaminate rapidly when heated in air, making the usual quenching technique of heating in air and plunging into a suitable liquid inapplicable. In 1963, a technique was developed by Rinderer and Schultz^{29/} which permits these metals to be annealed and quenched in the ultrapure conditions which exist in and directly above superfluid helium. They showed that fine wires could be resistance heated and quenched in the superfluid. This technique is used in the present experiment, which is the beginning of a planned systematic study of vacancies quenched into the refractory bcc metals (groups IVB and VB in the periodic table). Thus, a

TABLE 2
SUMMARY OF PAST WORK ON MOLYBDENUM

Investigator (s)	Method of Producing Vacancies	Temperature at which Vacancies Become Mobile (K)	E_m^V (ev)	E_f^V (ev)	Q (ev)	Ref.
R. Martin (57)	cold work	430	1.26			30
H. R. Peiffer (58)	cold work	420				32
G. H. Kinchin & M. W. Thompson (58)	neutron irradiation	420	1.3			11
E. V. Borisov, P. L. Gruzin, L. V. Pavlinov, G. B. Fedorov (59)					5.0	31
Von W. Danneberg & E. Krautz (61)					4.37	33
J. Nihoul (62)	neutron irradiation	Stage III not				
J. Nihoul (62)	quench	vacancies 700				25
D. E. Peacock & A. A. Johnson (62)	neutron irradiation	Stage III, 430	1.25			34
J. Askill (63)					4.0-4.2	35
Ya. A. Kraftmakher (64)	specific heat extrapolation			2.24		26
J. D. Meakin, A. Lawley, R. Koo (64)	quench in molten indium			2.5		24
C. P. Flynn (68)	----theoretical calculation----		2.2			22

large part of the experiment consisted of the design, construction, and testing of the apparatus to be used. In this thesis the apparatus and technique for superfluid quenching are described in detail, and new experimental results on quenched tungsten and molybdenum are presented.

To check out our apparatus, we first performed fast quenches on tungsten in an attempt to reproduce Schultz's data. We also studied how the quenched-in resistance varied as a function of quench speed to investigate vacancy loss during the quench, and to test Flynn's theory of vacancy annealing during the quench.

We then performed isochronal anneals on quenched tungsten specimens to see whether the quenched-in resistance recovered in a single annealing stage. This data was analyzed using first and second order kinetics to get an estimate of the effective motion energy for comparison with cold work and radiation damage experiments. Isothermal anneals with change-of-slope measurements were performed to get another, presumably more reliable, estimate of the effective motion energy. Preliminary experiments on vacancies quenched into molybdenum are also described.

II. QUENCH TECHNIQUE

A. Specimen Preparation

The tungsten specimens used for all of the quantitative data reported here were obtained from Westinghouse Electric Corporation. They were fabricated from highest purity zone-refined single crystal tungsten rods which had a guaranteed resistance ratio of at least 30,000 and typically 60,000. These rods were drawn to 2, 1.5, 1.2, and 1.0 mil wires by Westinghouse.

We first gave the as-received wires a short pre-anneal of 1/2 to 1 minute at 950-1000K in a vacuum of 10^{-5} Torr or better, to remove the "springiness" from them, making them easier to work with. The wires were then mounted on holders described below. The specimen, which was about 3 inches long with gauge length of about 1 inch, was supported by 10 mil platinum current leads. The potential leads were of 1/2 mil Westinghouse HRE Grade tungsten. For the earliest specimens, the potential leads were merely spot-welded to the specimen. However, we had trouble with these spot-welds breaking loose. To avoid this problem, most of the later specimens for which data were obtained had the potential leads tightly tied on with the knot spot-welded in place. Occasionally these leads broke loose from the specimen, in which case they were spot-welded back in place. For the later annealing studies we used 0.3 mil (General Electric #218 EES tungsten) potential leads, spot-welded on, to minimize temperature variations along the specimen.

The resistance ratio of the wires at this time was about 10. The earlier specimens were then annealed above the superfluid helium, within a few centimeters of the surface. The specimens were resistance heated to about 3000K for 5-15 minutes, then cooled in about 300 degree steps of 1-2 minutes each until the specimen temperature was down to about 800K, after which it was quenched. The base resistance was then measured. This procedure was repeated until the base remained constant to within one per cent. The total time at 3000K was usually about 1/2 hour. After this anneal the resistance ratio was in the range 600-650 for the 1.0 mil specimens and 700-750 for the 1.2 mil specimens. This annealing technique required several liters of helium per specimen, and constant attention to keep the specimen within a few centimeters of the superfluid surface.

Several attempts were made to anneal specimens in a vacuum of 5×10^{-6} Torr instead of over the superfluid helium with resulting resistance ratios anywhere between 50 and 550. After a short helium anneal these ratios increased to the same range as those given above for the helium anneals. The later tungsten specimens were given a wet hydrogen anneal. The specimen was placed in a NRC evaporator, which was evacuated to about 10^{-6} Torr. Commercially pure hydrogen was then passed over distilled water and allowed to bleed into the evaporator so as to maintain a pressure of 2 to 3×10^{-4} Torr. The specimen was then resistance heated to 2700-2800K for several hours, and cooled in 300 degree steps of 1-5 minutes each until the specimen was down to room temperature. This procedure yielded resistance ratios in the range 400-650. Short superfluid helium anneals (5 minutes at 3000K) increased this ratio to the same range, or slightly higher (up to 850 for some 1.2 mil specimens),

than the helium anneals on the earlier specimens. Apparently the hydrogen combined with some of the impurities and formed volatile compounds which were carried away with the hydrogen flow.

The molybdenum specimens were also obtained from Westinghouse. They were fabricated from highest purity molybdenum and were drawn to 1.5 and 1.1 mil wires. These wires were not given a pre-anneal. Short anneals above the superfluid (6 minutes) resulted in a stable base resistance, hence the molybdenum specimens were annealed only above the superfluid. The details of the annealing of the molybdenum specimens are described in the discussion of the molybdenum results.

B. Quenching Procedure

1. Room temperature Measurements

Before each experiment (and several times during the experiment) each specimen was placed in a draft-free plexiglass box where its room temperature resistance was determined by passing a small known current (typically one milliampere) through the specimen and measuring the voltage drop across the gauge length. The resistance at 273K was then calculated from the formula,

$$R_{273} = \frac{\Delta R(T)}{1 + \alpha \Delta T},$$

where $R(T)$ is the resistance at room temperature, ΔT is the difference between room temperature and 273K, and α is the temperature coefficient of resistivity taken as $4.5 \times 10^{-3} \text{ (K)}^{-1}$ for tungsten. To cancel the effect of the specimen geometry from the data, all measured resistances were divided by R_{273} .

2. Lighting Procedure

The specimen was placed in the cryostat and lowered to within about two inches of the surface of the superfluid helium. Since the specimen was then approximately at liquid helium temperature, its resistance was several hundred times lower than its room temperature resistance. Large current was required to put enough energy into the low resistance specimen to cause it to heat. However, as soon as the specimen started to heat appreciably, its resistance increased very rapidly. The current then had to be rapidly decreased, to keep the specimen from burning out.

To do this we discharged a capacitor through the specimen. Figure 2 is a simplified schematic of the circuit used. The power supply was adjusted to pass a current through the specimen sufficient to keep it heated once it was lit. Of course, this current was much too small to light the cold specimen. The 120 microfarad capacitor which had been charged by the charging circuit, was then discharged through the specimen by closing S_1 . This impulse current was made high enough to instantaneously heat the specimen; the heating current already passing through the specimen then kept it lit. The impulse current could be changed by varying either the capacitance or the charging voltage across the capacitor. For this experiment the 120 microfarad capacitor was charged to a voltage of 10 to 50 volts depending on the particular specimen. The diode was used to keep the impulse from being shorted by the power supply. The power supply must be a constant current source rather than a constant voltage source because it must supply approximately the same current both when the specimen is heated and when it is cold. The power supply we used was a Kepco model KS-60, which could operate either in constant voltage or

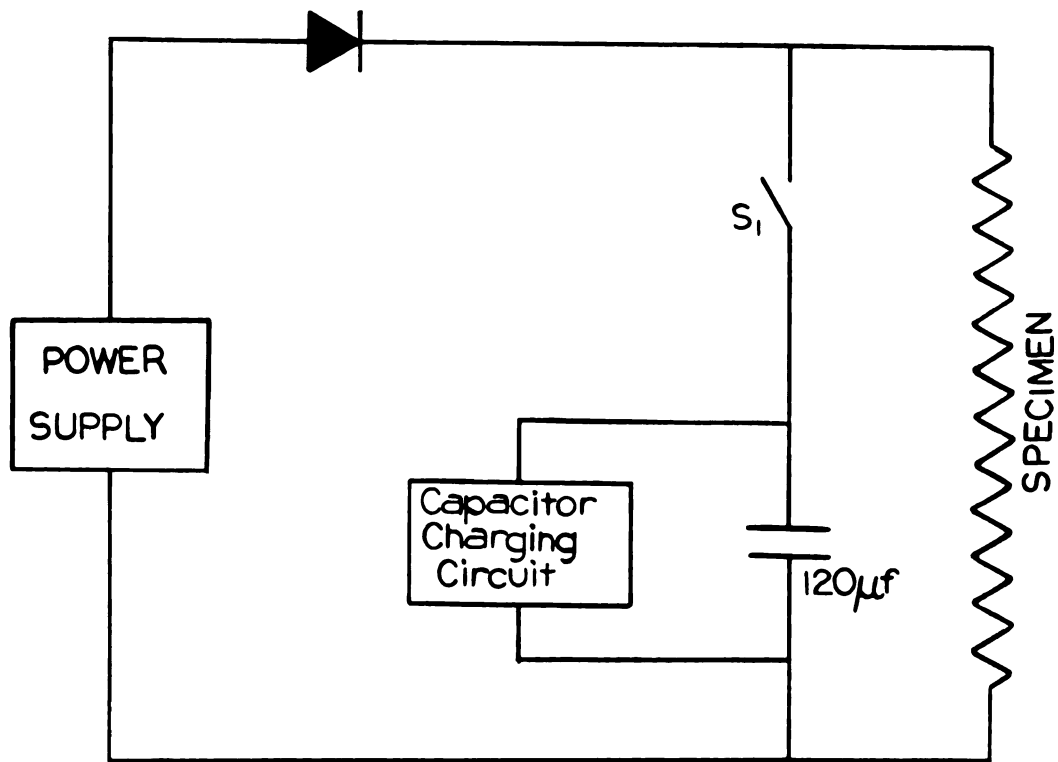


Figure 2: Simplified Schematic of the Capacitance Discharge Circuit

constant current mode. We adjusted the power supply so that it was in constant current mode until the specimen lit, at which time it automatically shifted to constant voltage mode. This was done because the specimen's temperature could be controlled more easily by controlling the voltage across it rather than the current through it.

When a specimen was first lit, it usually had a "hot spot" 1/8 to 1/2 inch long. The voltage across the specimen then had to be slowly and carefully increased until the hot spot spread across the whole specimen. It was much easier to light the specimen after it had once been uniformly glowing above the superfluid. Presumably this was due either to a surface effect or some local defect which annealed away during the first superfluid anneal.

3. Temperature determination

After the specimen was uniformly glowing, it was heated to the desired temperature by increasing the voltage across it. The temperature was determined from the ratio $R(T)/R_{273}$, where $R(T)$ is the resistance at the temperature T and R_{273} is the resistance of the same specimen at 273K. The resistance ratio versus temperature data of the National Bureau of Standards ^{36/} (NBS) was used to determine the temperature. *

When the temperature had to be known accurately, for example, immediately before a quench, the direct current and voltage were determined with precision potentiometers. When the temperature of the specimen had to be known only to a few per cent, as for anneals and for

^{37/}
*The data of Langmuir and Jones (which Schultz used) do not agree with this data. They differ by approximately 60 degrees in the range 2000 to 3200K. We have adjusted Schultz's data to the NBS temperature scale for comparison with our data. We have also changed Schultz's data from resistivity to resistance using the formula: $R(T)/R_{273} = \rho(T)/\rho_{273}$, where ρ_{273} was taken to be $5.055 \mu\Omega \text{ cm}$.

attaining the approximate temperature before a quench, alternating current (AC) circuits (described in Section III C. 2.) were used to find the resistance ratio (hence temperature).

4. Quenching under the superfluid

The specimen is usually lit and annealed about an inch above the superfluid. For a quench the lit specimen is lowered into the superfluid. If one watches the specimen pass through the surface one sees essentially nothing happen; as near as one can tell by eye the temperature of the specimen doesn't change and the superfluid remains calm. As the specimen is lowered through the surface, a thin gaseous layer of helium forms around the wire to insulate it from the superfluid. The superfluid conducts the heat away from the gaseous layer so well that no gas bubbles form around the specimen. Also, when the specimen passes through the surface of the superfluid the current changes only slightly, indicating that the energy dissipated by the specimen is very nearly the same in the superfluid as it is in the low pressure helium gas just above the surface. During a typical experiment the pressure above the liquid helium is 1 to 5 Torr. At these pressures the helium gas is a poor heat conductor, hence the energy is dissipated almost entirely by radiation. This is confirmed by the fact that nearly the same energy (within a few per cent) is dissipated when the specimen is heated to a given temperature in a vacuum of 10^{-6} Torr, as when it is heated to the same temperature in the superfluid. The fact that the liquid helium is a superfluid is not critical;* only the low pressure above the liquid helium is important to keep the heat loss by gaseous

*See Appendix A for further discussion of the significance of the superfluid.

convection currents to a minimum. If the helium pressure rises above a few centimeters of mercury, the temperature uniformity along the specimen becomes variable and very poor.

After the specimen was immersed in the superfluid, and the quench temperature determined, the specimen was quenched. For fast quenches, the heating current was abruptly turned off. Slower quench speeds were obtained by merely connecting a capacitor in parallel with the specimen and allowing the capacitor to discharge through the specimen after the power supply was disconnected. By varying the capacitance we could conveniently vary the quench speed as needed.

5. Determination of the helium temperature resistance

After the specimen was annealed or quenched, its resistance was measured at liquid helium temperature. The "measuring circuit" (described below) was used to pass a known direct current (typically either 1 or 1/2 ampere) through the specimen while it was immersed in liquid helium. This current was determined by measuring the voltage drop across a 1 ohm standard resistor in series with the specimen. Both this voltage and the voltage across the gauge length were measured with precision potentiometers. For both room temperature and base resistance measurements, reversing procedures were used to cancel the effects of any slowly varying thermal voltages.

6. Advantages and disadvantages

The superfluid helium quenching technique has several advantages over conventional quenching techniques. 1) The specimen is in a pure helium atmosphere at temperatures so low that all other gases are solid.

2) Since the specimen is quenched in situ, it is not strained or deformed as in water quenches. 3) The specimen is quenched directly to liquid helium temperatures so that the quenched-in resistance can be measured immediately. 4) The quench speed can be conveniently varied by simply allowing a capacitor to discharge through the specimen. The main disadvantage of the technique is that very fine wires or foils must be used to keep the quench speed high and to keep the helium consumption low. Another disadvantage is that thin specimens do not glow uniformly at temperatures lower than about 1500K, limiting use of the technique to high melting metals.

III. APPARATUS

A. Specimen Holder

The specimen holder is drawn to scale in Figure 3. It consists of an 1/8 inch thick teflon sheet to which a 20 mil tungsten or galvanized steel sheet is attached. Teflon is used because it is an electrical insulator and is easy to work with. The specimen is mounted on the metal sheet so that expansion and contraction of the holder relative to the specimen will be minimized when they are cycled between room temperature and liquid helium temperature. After annealing, the specimens are quite brittle, and differential contraction between the specimen and the holder will break the specimen. The steel holders were much easier to make than the tungsten holders, hence, steel was used after it was decided that it worked as well as the tungsten. The large holes in the teflon reduce the mass of teflon so that less helium is used in cooling the specimen holder. The 10 mil platinum current leads are passed through a narrow hole in a nylon screw and threaded teflon post as shown in the figure. A nylon set screw holds the current lead in place. The specimen is spot-welded to the 10 mil platinum current leads. The 0.5 mil or 0.3 mil tungsten potential leads are spot-welded to the 10 mil platinum which is fastened to the holder under a washer and screw as shown in the figure. Platinum is used because it is a high melting metal which is easy to work with and which spot-welds well to tungsten. Copper wire is spot-welded

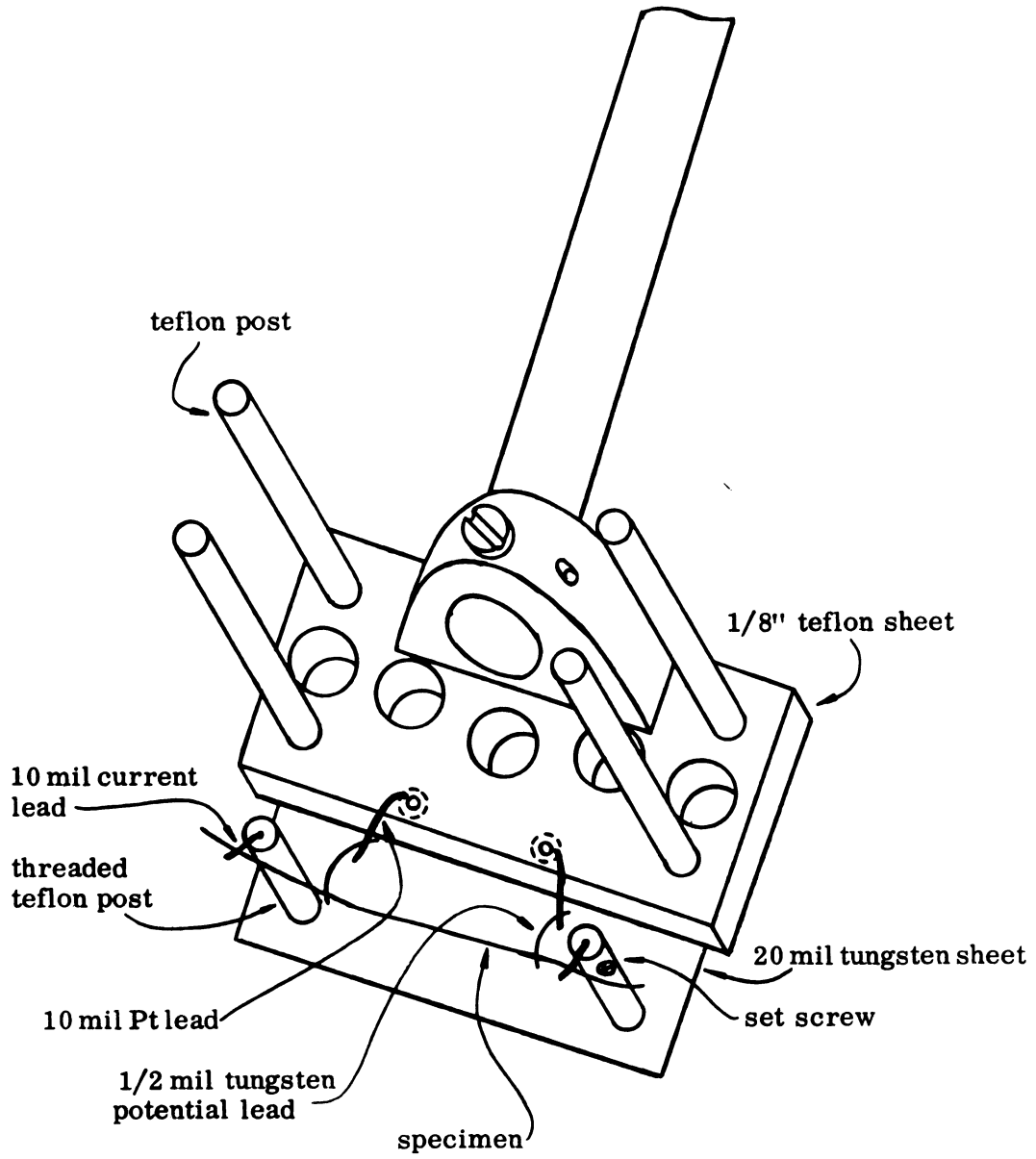


Figure 3 Specimen Holder

to the current lead and connected to a plug. The four long teflon posts are used to protect the specimen from hitting the sides of the dewar and to keep the specimen holder from banging around in the dewar as the specimen is raised and lowered.

B. Cryostat

Figure 4 shows the cryostat and associated equipment. The cryostat is a standard double dewar with a 3-1/4 inch diameter helium dewar. The outer dewar has two 1/2 inch wide viewing strips; the inner dewar has two 1-1/4 inch wide viewing strips. Above the dewar is a collar to which the main helium pump and manometers are connected. The pump is a Stokes Microvac model 212-H. With this pump we can obtain pressures of about one Torr above the liquid helium. On top of the collar is a CVC type VCS 41B, four inch diameter clearance, gate valve.

Above the gate valve is the "annealing chamber", which served as an air lock to get specimens in and out of the partially evacuated dewar. This chamber was also going to be used to anneal specimens in vacuum or in a gas, but the NRC evaporator became available and was used instead.

The specimen holder is supported by a 6 foot long, 1/2 inch diameter, thin-walled German silver tube. Current leads consisting of a twisted pair of #26 gauge insulated copper wire, and potential leads consisting of a twisted pair of #30 gauge insulated copper wire were passed down the center of this tube. To minimize thermal voltages in the circuit, the copper leads were continuous from the plug which mated to that on the specimen holder to a similar plug at room temperature. During measurements the lower plug was submerged in liquid helium and the room temperature plug was shielded from drafts by foam rubber. At the top of the tube the leads passed

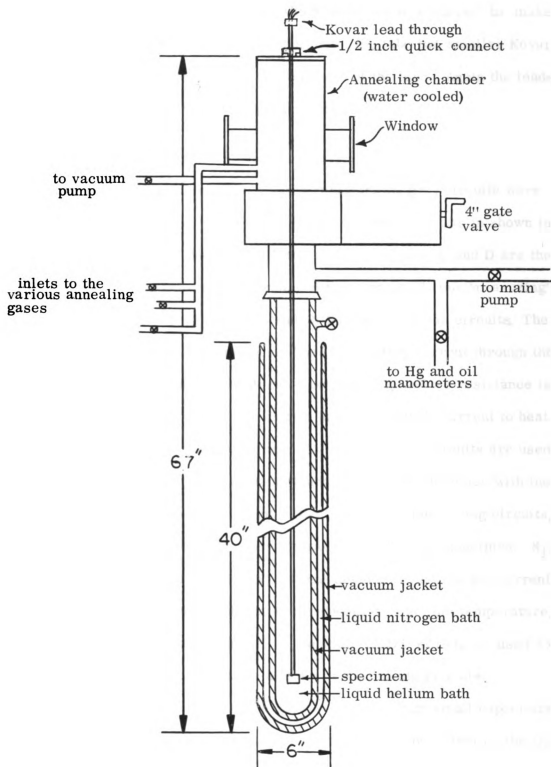


Figure 4 Cryostat

through Kovar "lead throughs" to which they were soldered to make vacuum-tight connections. Near the bottom of the tube two smaller Kovar "lead throughs" were used to get the leads out of the tube. Again the leads were soldered to make vacuum-tight connections.

C. Circuits

Both alternating current (AC) and direct current (DC) circuits were used in this experiment. A block diagram of these circuits is shown in Figure 5. A and B are the current leads to the specimen; C and D are the potential leads. The DC circuits consist of three parts: 1) the "measuring" circuits, 2) the "heating" circuit, and 3) the DC potential circuits. The "measuring" circuit is used to pass a known, constant current through the specimen when its room temperature or helium temperature resistance is being determined. The "heating" circuit is used to supply current to heat the specimen to various temperatures. The DC potential circuits are used to measure the voltage drop across standard resistors in series with the specimen to determine the current in the heating and measuring circuits, and to measure the voltage across the gauge length of the specimen. S_1 , a double pole, double throw (DPDT) switch, is used to reverse the current through the specimen when obtaining the specimen's helium temperature, or room temperature resistance. S_2 , another DPDT switch, is used to connect the specimen to either the heating or measuring circuits.

The AC circuits are connected to the specimen through small capacitors (about 0.01 microfarad); hence they have no measurable effect on the DC circuits. Each of these circuits will now be discussed in detail.

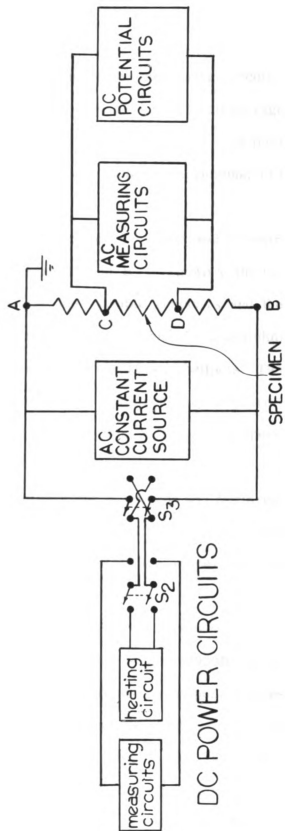


Figure 5: Block Diagram of Circuits

1. DC circuits

a. Measuring circuit

Figure 6 is a schematic of the measuring circuit. For the earlier experiments the power supply was a set of 6 volt storage batteries. Now a Princeton Applied Research (PAR) model TC 602R power supply is used. The output voltage of this power supply is more constant than the output of the batteries.

R_v is a series of resistors and switches used to control the measuring current. A detailed schematic of R_v is shown at the bottom of Figure 6. By appropriately varying the variable resistors and the switches, R_v is nearly continuously variable between 1 ohm and 52,221 ohms. The 1 kilohm and 50 kilohm variable resistors are 10-turn helipot. The fixed resistors are used to protect the variable resistors when they are turned to low resistance. With this system we can control a 1 ampere current to five places.

The 1 ohm standard resistor is a Leeds and Northrup National Bureau of Standards type resistance standard #4020B. It is used to measure the current when the specimen's liquid helium temperature resistance is being determined.

The 100 ohm standard resistor is a Leeds and Northrup National Bureau of Standards type resistance standard #4030B. It is used to measure the low current used in measuring the room temperature resistance. Whenever currents above a few milliamperes were used, the 100 ohm standard was shorted by S_3 to avoid damaging it and to decrease the resistance of the measuring circuits. The standard resistors are both four-terminal resistors; the potential terminals are connected to the potential circuits as indicated.

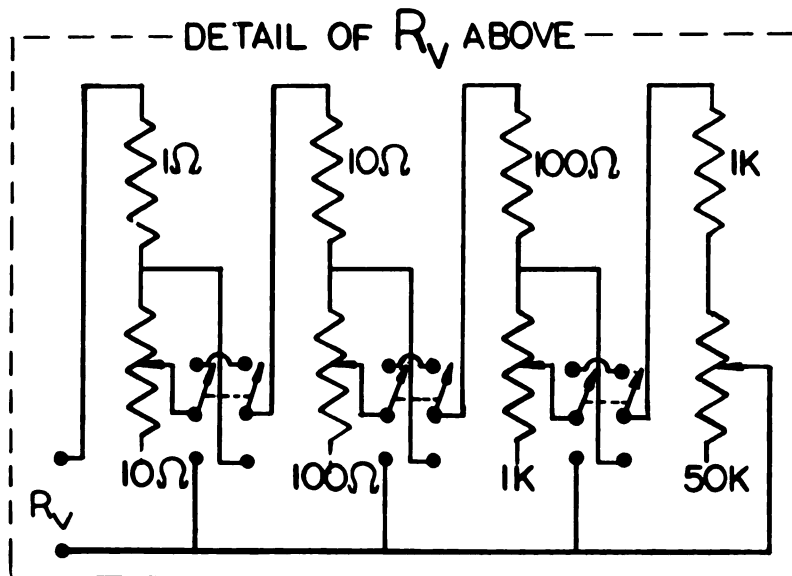
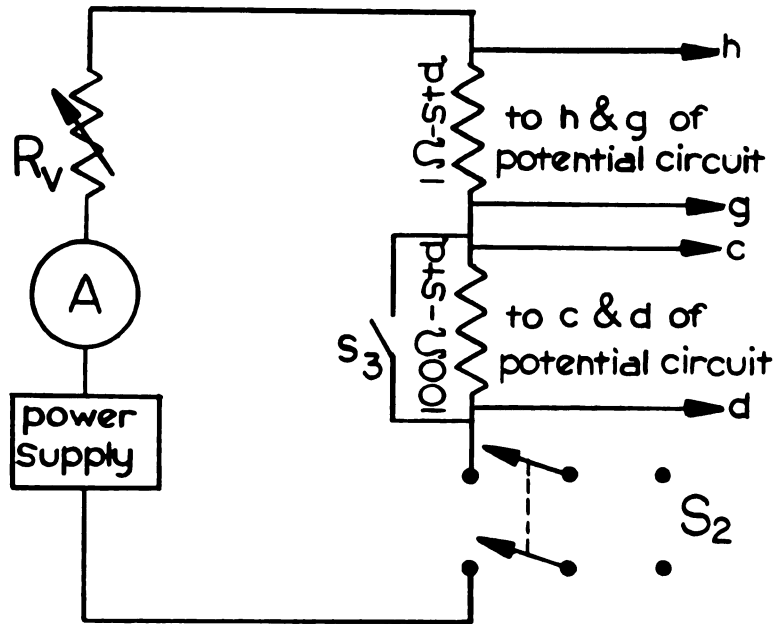


Figure 6: Measuring Circuit

b. Heating circuit

Figure 7 is a schematic of the "heating" circuit. The power supply is a Kepco model KS-60M power supply which can operate either as a constant voltage or a constant current source. For large currents (0.1-10 amperes) the 0.001 ohm shunt is used to determine the heating current. For the lower currents, used in the tungsten annealing experiments, typically a few hundredths of an ampere, the 0.02 ohm shunt is used. Both of these shunts are four-terminal resistors with their potential terminals connected to the potential circuits as indicated. They were both accurately calibrated against the 1 ohm standard in the measuring circuit. Switch S_4 is used to disconnect the 0.02 ohm shunt and other components in this branch from the circuits when the higher currents are used for other experiments; for all the experiments reported here this switch was positioned as shown. The 2 ampere fuse is used to protect the low current branch if S_4 is in the wrong position and high currents are used.

The 4 millihenry inductor and the 0.25 microfarad capacitor form a parallel tuned circuit to keep the AC circuits from being shorted by the quench speed capacitors and the power supply. The diode is used to keep the current impulse used to light the specimen from discharging through the power supply as discussed above. S_5 can be used to short the diode; for the present experiments it was always left open.

Switch S_6 is used to disconnect the power supply and let the quench speed capacitors discharge through the specimen as described earlier. Figure 8 is a schematic drawing of the quench speed capacitors. With this circuit, the capacitance can be varied from zero to 4100 microfarads in twelve steps.

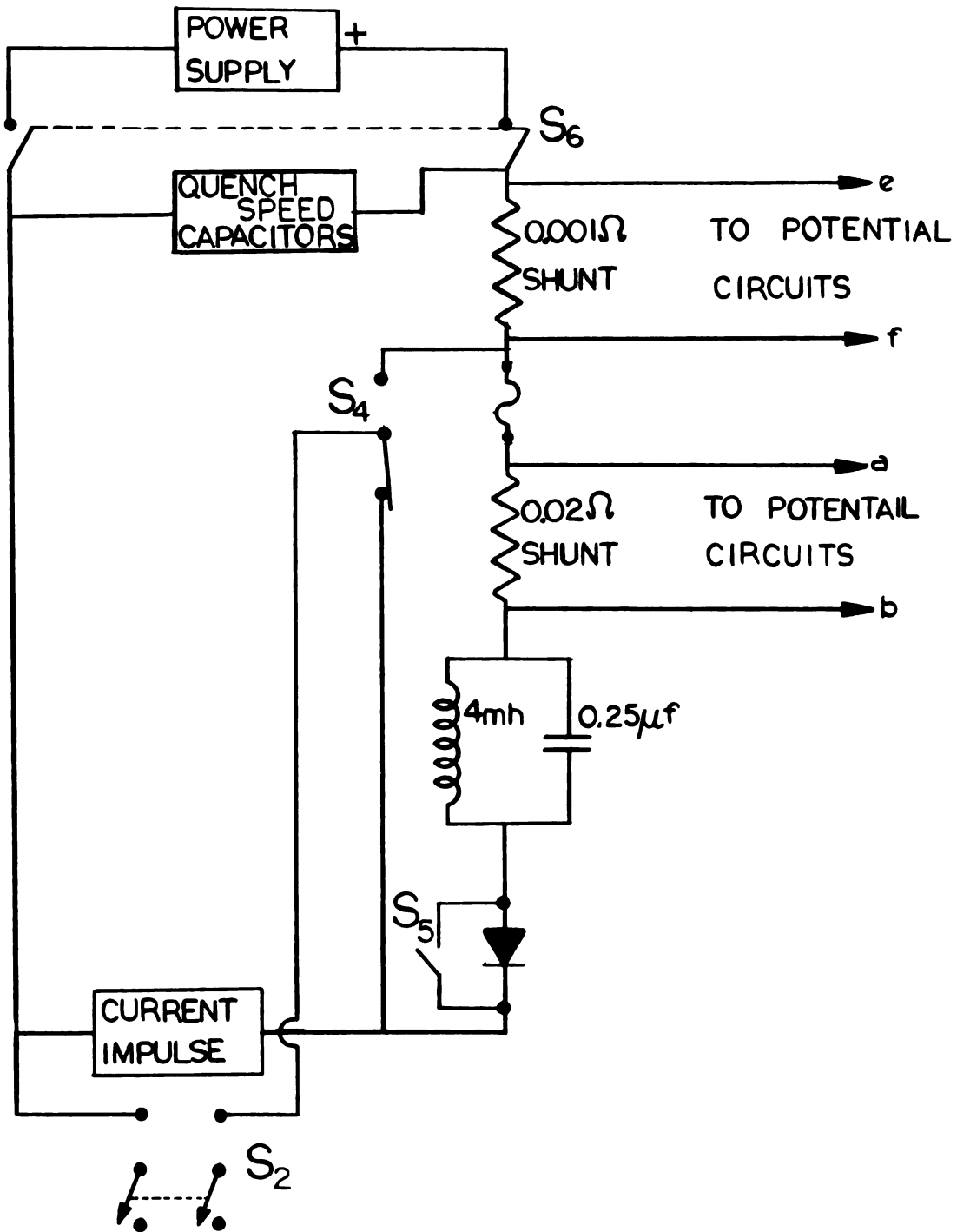


Figure 7: Heating Circuit

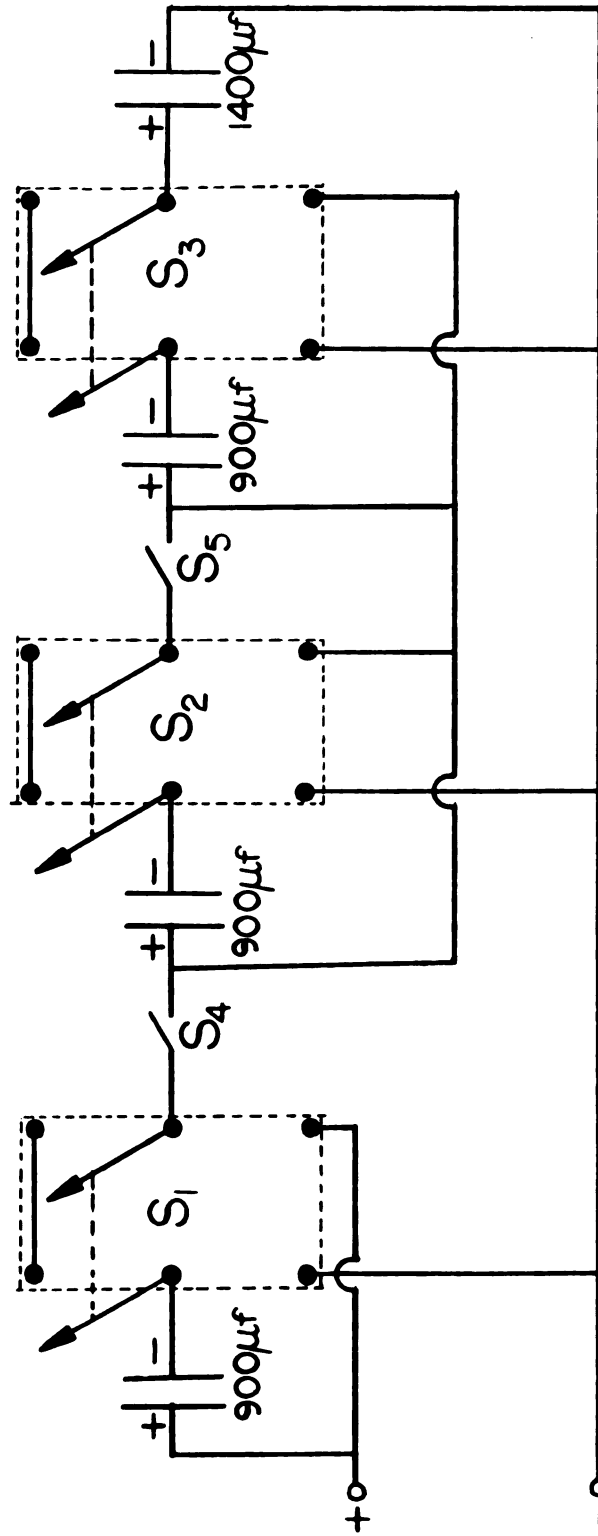


Figure 8: Quench Speed Control Capacitors

Figure 9 is a schematic drawing of the capacitor charging circuit which is used to light the specimen. T_1 is an isolation transformer; T_2 is an autotransformer. The meter is calibrated to read the charging voltage (0-100 volts). The 1 kilohm resistor limits the charging current. The 10 kilohm resistor is connected directly across the capacitor terminals to insure that it discharges when the system is turned off. It also allows the capacitor to discharge faster if the Variac output voltage is decreased (i.e., it decreases the time constant RC of the 120 microfarad capacitor). S_7 is a single pole, single throw, spring loaded open switch used to discharge the 120 microfarad capacitor through the specimen.

c. Potential circuits

Figure 10 is a diagram of the potential circuits. Switches S_8 and S_9 are double pole, twelve position switches made by Grayhill (number 44D30-02-1-ADJ-N). These switches are connected in parallel so that either of the potentiometers can be used to read the potential of interest.

Potentiometer A is a Honeywell model 2780 with a Leeds and Northrup DC Null Detector (No. 9834). Potentiometer B is a Honeywell model 2779 microvolt potentiometer. A photocell galvanometer amplifier (type 5214/9460) and a secondary galvanometer (type SR21/9461), made by Guildline Instruments Limited, are used as a null detector for this potentiometer. The reversing switch preceding the microvolt potentiometer is a Honeywell model 3565 thermal-free reversing switch. It is used to reverse the potential when the current through the specimen is reversed during room temperature and helium temperature resistance measurements.

The letters "a" through "h" correspond to the same letters on the standard and shunt resistors in the measuring and heating circuit diagrams;

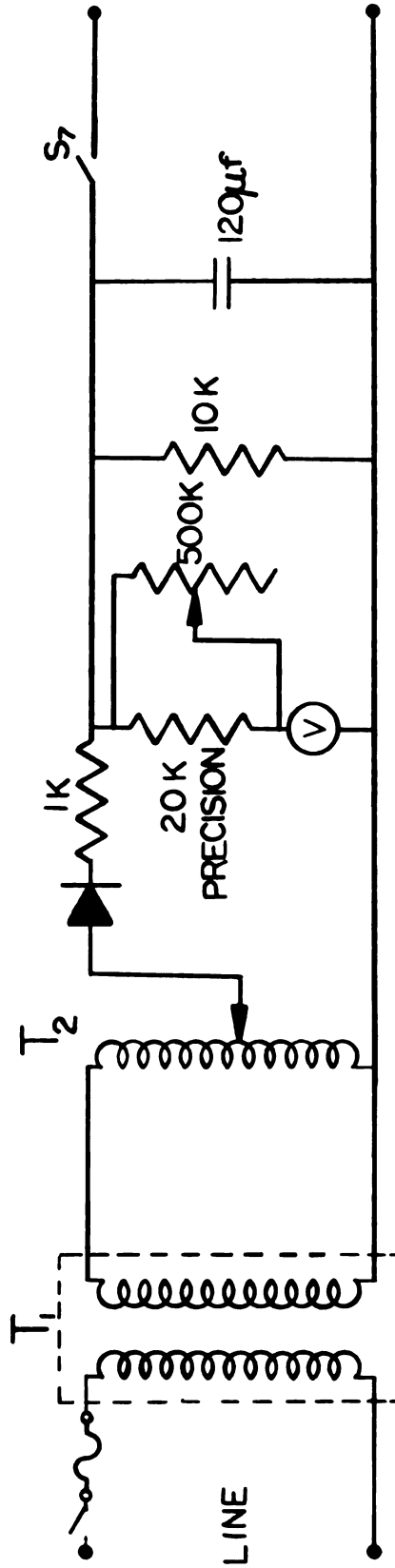


Figure 9: Capacitor Charging Circuit

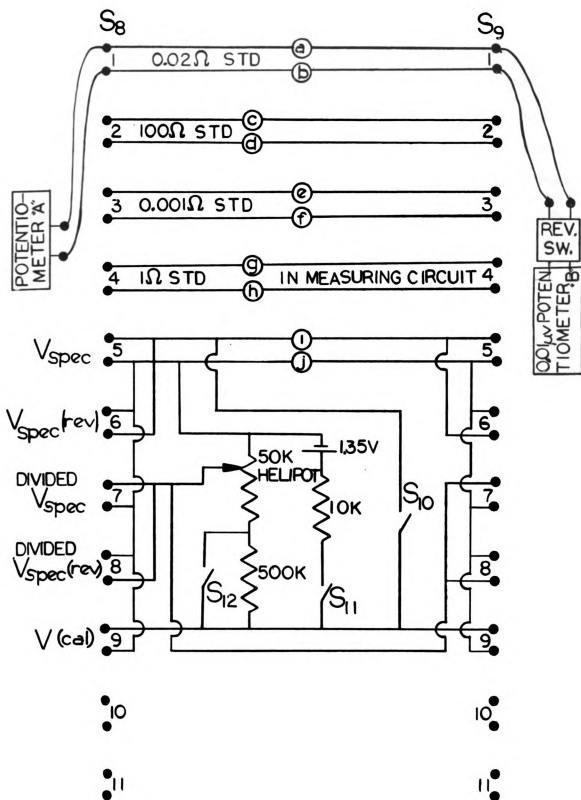


Figure 10: Potential Circuits

"i" and "j" connect to the potential leads of the specimen. These account for the first five positions of the switches. Position 6 reverses the potential leads to the potentiometers.

When the specimen is heated, the voltage across the gauge length is on the order of ten volts. Since this is too large for the potentiometers to measure, the voltage divider shown in the lower part of Figure 10 was designed and built. Voltages as high as several hundred volts can be measured with this circuit and a potentiometer capable of reading 1.5 volts. For the present experiments switch S_{12} is always closed, shorting the 500 kilohm resistor and permitting a voltage ratio of ten to be used.

Before using the voltage divider circuit it must be calibrated. This is done by first opening S_{10} to disconnect the specimen and closing S_{11} which connects the mercury cell into the circuit. Potentiometer A is then switched to position 9 and the voltage measured. This voltage is then divided by the desired ratio, potentiometer A is turned to position 7 and the 50 kilohm helipot adjusted until the potentiometer measures the divided voltage. The 50 kilohm helipot is then locked into place, and the readings checked again. S_{11} is then opened and S_{10} closed. The specimen voltage divided by the ratio is then measured by measuring the potential at position 7.

Potentiometer A is used to measure the voltage across: the 100 ohm standard for room temperature resistance measurements; the 1 ohm standard for helium temperature resistance measurements; and the gauge length of the specimen when it is heated. Potentiometer B is used to measure the voltage across the gauge length of the specimen for room and helium temperature resistance measurements, and across the 0.02 ohm or 0.001 ohm shunt resistor for high temperature resistance measurements.

2. AC circuits

Since the specimen's temperature is changed by varying the direct current through it, the DC voltage across the gauge length of the specimen is not directly proportional to its resistance. For fast quenches the current is turned off, hence there is no DC signal across the gauge length during the quench, making it impossible to determine the quench speed directly. To avoid these difficulties a small, constant AC current of 5000 hertz (Hz) is passed through the specimen continuously during the experiment. The AC signal across the gauge length of the specimen is then directly proportional to its resistance, regardless of the direct current flowing through the specimen. This technique could also be applied to conventional quenching experiments, and would be especially useful for "air" quenches when the specimen is quenched by turning off the heating current. Figure 11 is a block diagram of the AC circuit. It consists of four major sections: 1) a source of constant AC current which is passed through the specimen in parallel with the direct currents, 2) an AC amplifier, 3) an AC to DC converter, and 4) read out devices. To assist the reader in understanding these circuits, a brief description of operational amplifiers is given in Appendix B.

a. Constant current source

The AC constant current source drives a constant alternating current of several milliamperes through the specimen independent of the specimen's resistance. A schematic diagram for this device is shown in Figure 12. The generator "G" is a Hewlett Packard model 202C Audio generator. The operational amplifier is a Philbrick P65AU. It has an open loop gain of better than 20,000 and a maximum output of 2.2 milliamperes at 22 volts

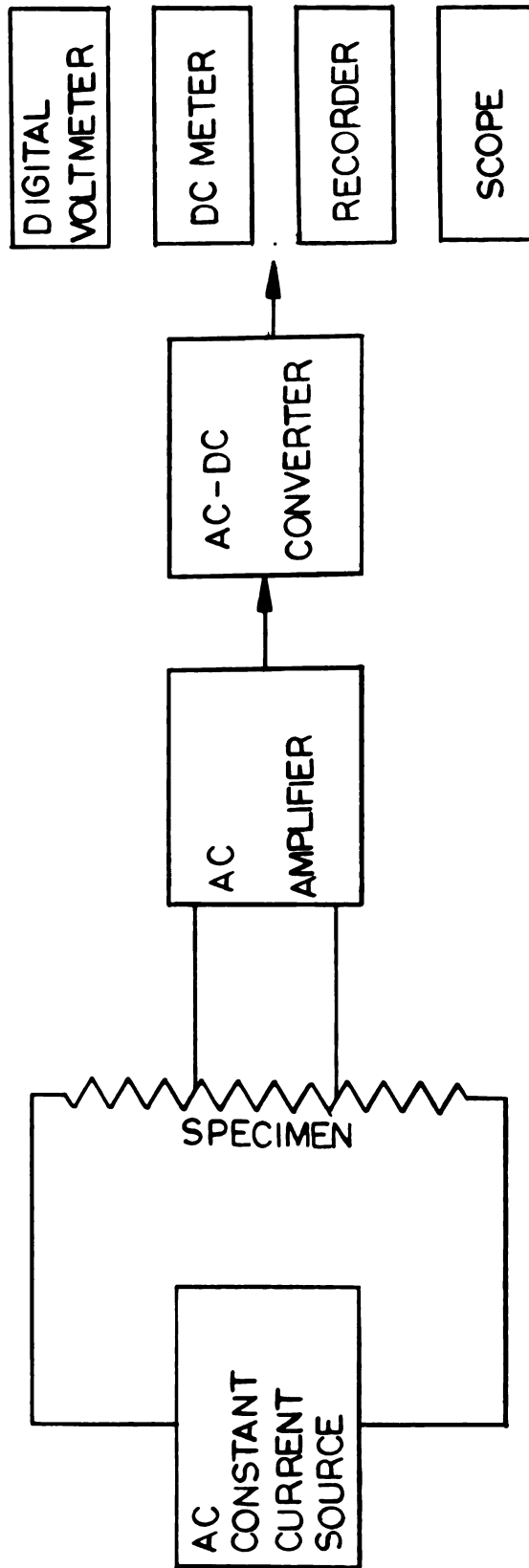


Figure 11: Block Diagram of the AC Circuits

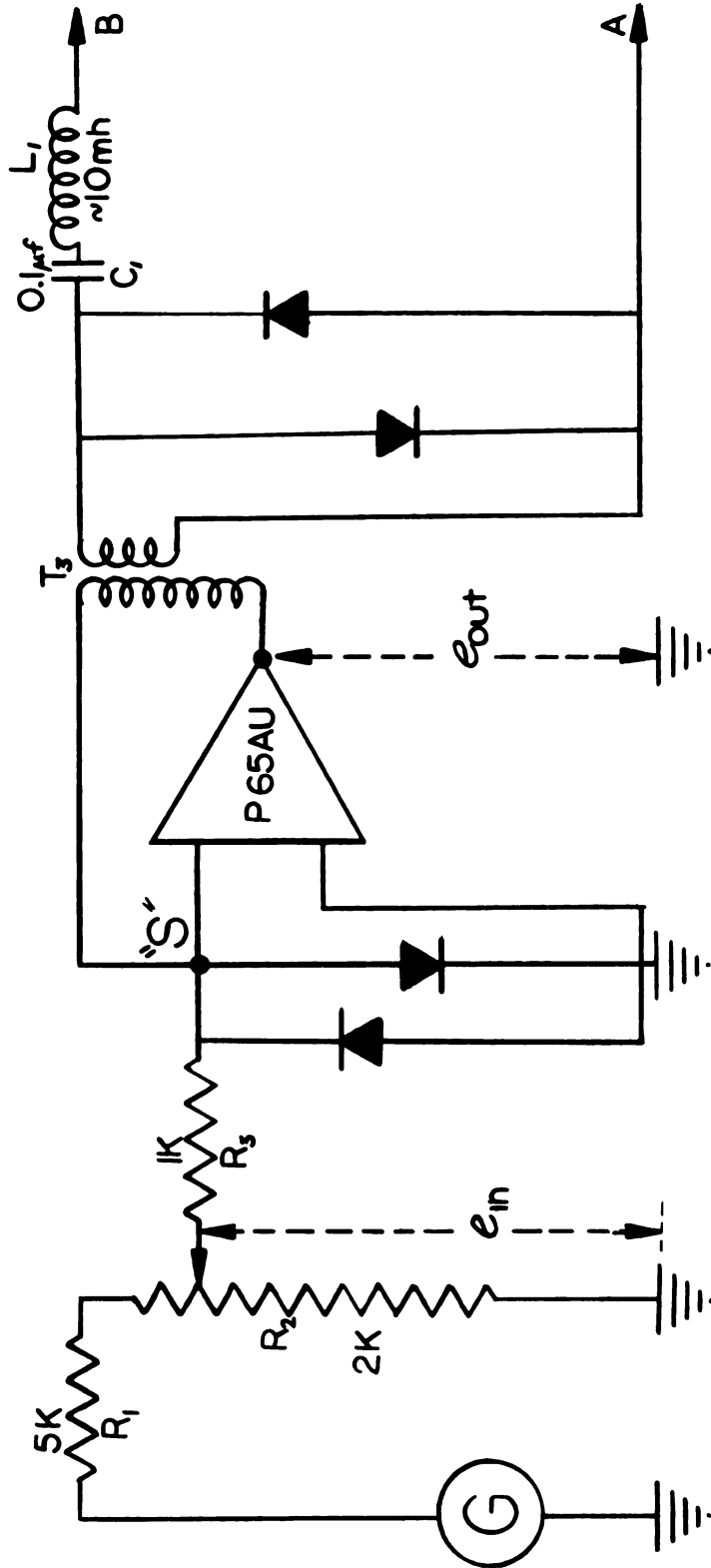


Figure 12: AC Constant Current Source

peak to peak. The diodes are Sylvania 485 silicon diodes; R_2 is a ten-turn helipot; T_3 is a filament transformer (117v. to 24v.).

R_1 and R_2 form a voltage divider which permits fine control of the voltage e_{in} . Since point 'S' is a virtual ground, the current input i_{in} is $e_{in}/1000$. As described in Appendix B this current flows through the primary of the coupling transformer T_3 regardless of the impedance seen by the secondary as long as the operational amplifier is not overloaded (i.e., it is a constant current source). T_3 is a step-down transformer used to match the impedance of the specimen to the operational amplifier. Since there is a DC potential between the points A and B, whenever a DC current is flowing through the specimen, a capacitor C_1 is placed in series with the secondary of the transformer to keep it from shorting the specimen. However, during a quench this capacitor must discharge through the specimen and T_3 . Hence, to get the fastest quenches and to minimize overloading of the operational amplifier, C_1 should be small. On the other hand, C_1 should be large enough to pass the AC with little impedance. This problem is solved by using the series tuned circuit (tuned to the operating frequency) consisting of C_1 and L_1 (assuming that T_3 is a "perfect" transformer and that the operational amplifier is "resistive").

The diodes are used to protect the operational amplifier. If the specimen breaks or is disconnected, the operational amplifier will still try to maintain a constant current. This would severely overload the operational amplifier if it were not for the diodes which conduct when the voltage rises above a few tenths of a volt. In normal operation the voltage across the diodes is at most a few millivolts; with a forward bias this small, the diodes have a very high impedance (essentially infinite).

B. Amplifier

Figure 13 shows a schematic diagram of the amplifying section of the AC circuit. T_4 is a United Transformer Company No. H-20 transformer. It must be capable of operating at 5000Hz and the resistance in the windings must be low since it is part of the input resistance of the operational amplifier. Also, it must be well shielded since it passes small signals and rather large stray fields are present. The capacitor C_3 is used only as an added safety to keep direct current out of the operational amplifier circuit. R_4 is the input resistor for the operational amplifier. The operational amplifier is a Philbrick P45AU. It has an open loop gain of 300,000 and a maximum output of 20 milliamperes at 20 volts peak to peak.

The transformer T_4 enables one side of the signal to be grounded. As above, capacitor C_2 is needed to block the direct current from the amplifier circuit. The AC signal is on the order of millivolts, whereas the DC potential is around ten volts before a quench. At the time of a quench the capacitor C_2 must discharge through the diodes and transformer. Since the diodes don't "turn on" until there is a few tenths of a volt across them, the amplifier is overloaded with a pulse more than a hundred times larger than the signal. For this reason C_2 must be kept as small as possible so that the pulse is over quickly, allowing the AC circuits to follow the resistance of the specimen as it cools. Many attempts were made to keep most of this pulse from the amplifier. The most successful was the series tuned circuit consisting of C_2 and L_2 as shown. L_2 blocks most of the pulse from the transformer thereby forcing most of it to flow through the diode. As in the constant current source the voltage across the diodes in normal operation is only a few millivolts, leaving them with essentially infinite impedance.

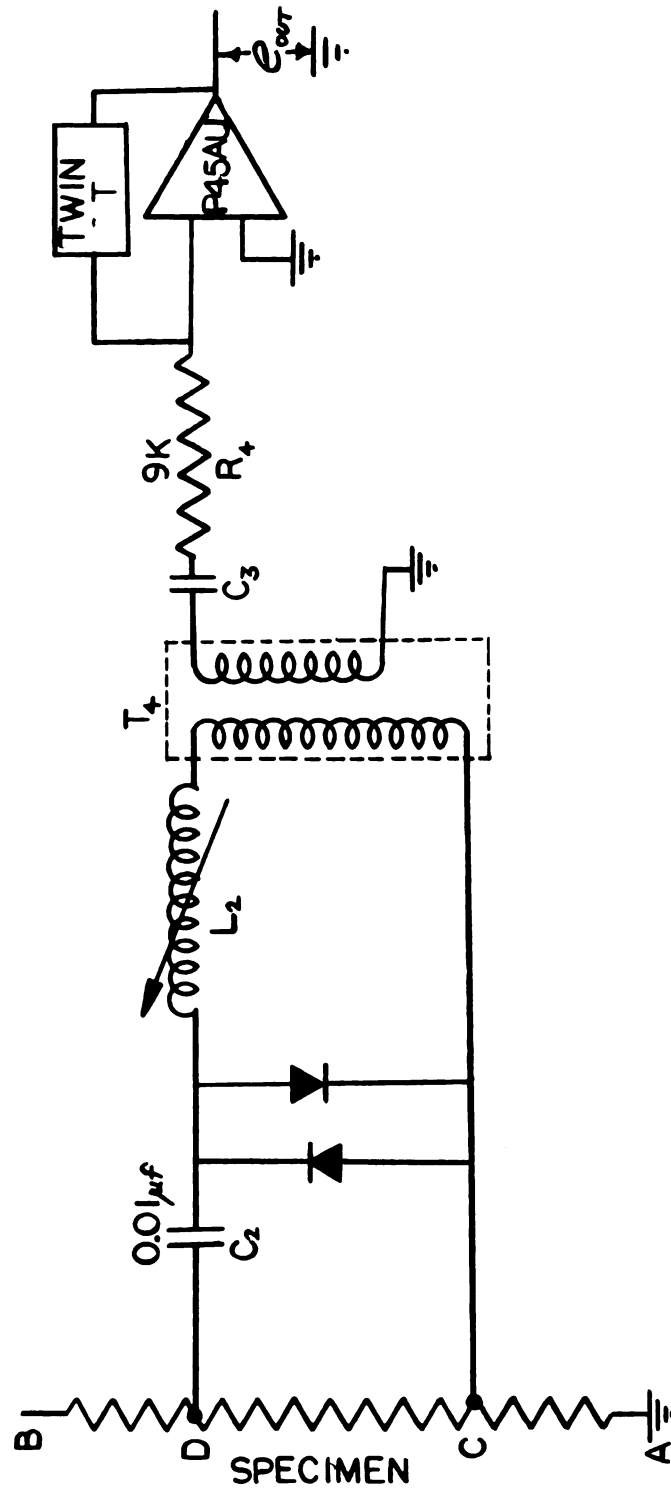


Figure 13: AC Amplifier

To decrease noise and to help remove the spurious pulse discussed above, a frequency-selective network was used for the feedback impedance. As discussed in Appendix B the gain of the operational amplifier is $\frac{R_f}{R_{in}}$. If R_f is small for all frequencies except a narrow band of frequencies, only this narrow band will be amplified by the amplifier. A twin T network is used for this purpose. It is called a twin T network because of the shape of its schematic (see Figure 14). The resonant frequency is given by $\omega = 1/RC$. The twin T network was made by carefully mounting precision components on a terminal strip. A 380 picofarad capacitor was used instead of a 360 picofarad (2 x 180 picofarad) because a 360 picofarad capacitor was not immediately available at the time. At the resonant frequency the impedance of the twin T was about 10 megohms. This network determines the operating frequency of the AC circuits.

c. AC to DC converter

The output of the amplifying circuit e_o is a 5000Hz signal whose amplitude is proportional to the resistance of the specimen. The circuit shown in Figure 15 is used to convert this signal to a DC signal which is directly proportional to the amplitude of the AC signal. T_5 is a 6:1 step-up transformer, which steps up the output voltage to the diodes. Since the diodes are not fully turned on below approximately 1/2 volt, non-linear response results if the AC signal is not much larger than this. The typical output of the operational amplifier is 10 volts peak to peak. With the 6-fold voltage increase, the diodes typically rectify 60 volts peak to peak, and the non-linearity in the first half volt is negligible. The 40 kilohm resistor is placed before any capacitors so that the diodes see a resistive load. If the filter capacitor were placed before the major resistance of the load,

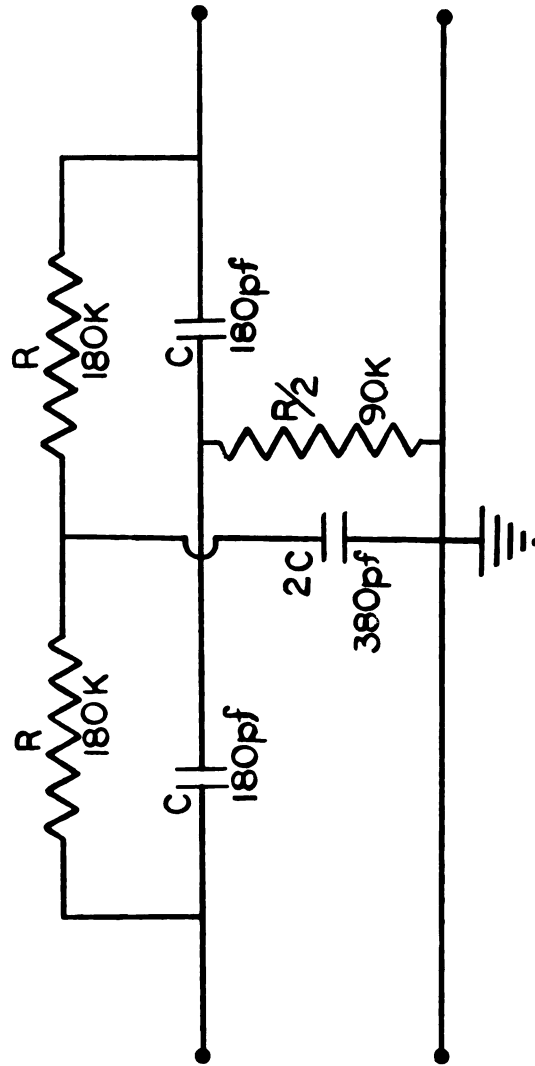


Figure 14: Twin T Network

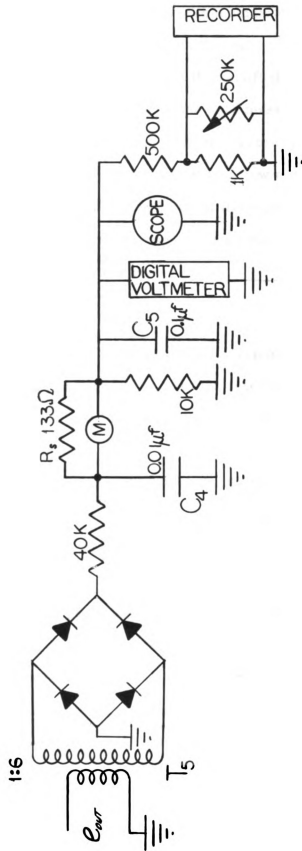


Figure 15: AC to DC Converter

the diodes would be turned on only a short time with a small voltage drop across them. See Figure 16 and accompanying discussion.

The capacitors C_4 and C_5 are used to smooth the rectified DC to provide nearly pure DC for the read out devices. Some care must be taken to use low values for these capacitors for two reasons: 1) to measure the quench speeds, the time constant should be less than a few milliseconds and, 2) the overloading pulse through the amplifier at the beginning of the quench should be quickly discharged from the capacitors so that the circuits can again indicate the specimen's resistance.

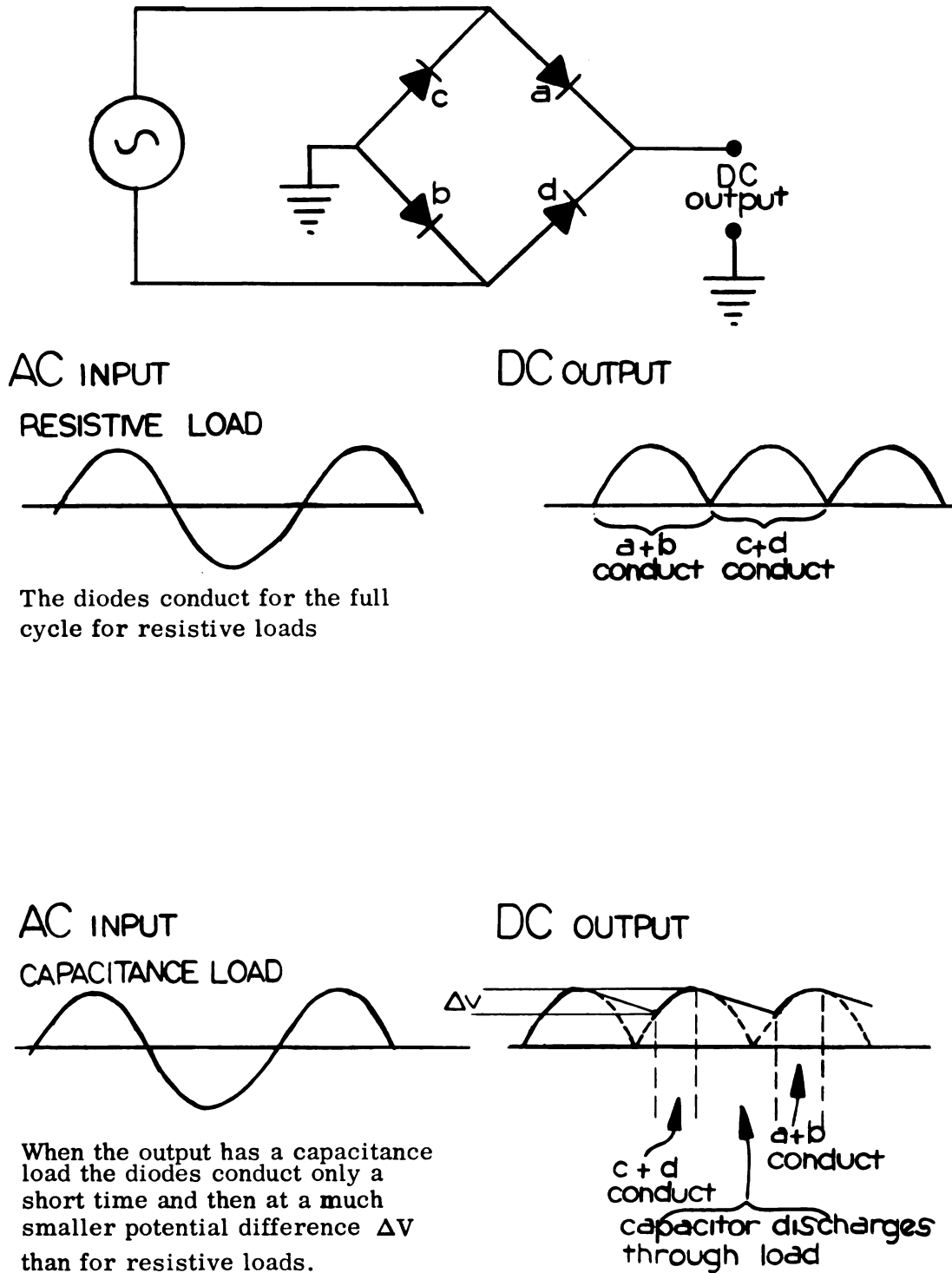
d. Readout devices

At this stage the signal is a DC voltage which is proportional to the resistance of the specimen. To "read" this signal four devices (connected as shown in Figure 11) are used; a DC meter, a digital voltmeter, a strip chart recorder, and an oscilloscope.

The DC meter is a Weston model 271 which reads full scale at 50 microamperes. The meter shunt resistor R_s is chosen to give full scale deflection when e_0 is nearly at the maximum output of the operational amplifier.

The digital voltmeter (Data Technology Corporation model 323) was acquired after most of the present experiments were finished. Its readings are accurate to within ± 0.01 per cent, much better than the DC meter. After calibration the AC circuits give the resistance ratio in the region of interest to within a few tenths of a per cent with the digital voltmeter; they were accurate to only a few per cent with the DC meter. The DC meter is now used only as a check on the output of the AC circuits.

The recorder is a Honeywell model 153X11V-X-28 strip chart recorder.



The diodes conduct for the full cycle for resistive loads

When the output has a capacitance load the diodes conduct only a short time and then at a much smaller potential difference ΔV than for resistive loads.

Figure 16: Diode Output to Resistive and Capacitive Loads

A voltage divider must be used at the recorder input because the recorder gives full scale deflection for 10 millivolts input. The recorder is used to record resistance of the specimen as a function of time during a run. The recorder chart then allows one to have for future reference a permanent record of: the temperatures at which the specimen was annealed and for how long it stayed there, the time the specimen was at the quench temperature before a quench was made, and any unexpected changes in the resistance of the specimen, e.g., when a specimen breaks or potential leads come loose.

The scope is a Tektronix model 531. It is used with a scope camera to provide pictures of the DC output as a function of time during a quench. The scope is triggered by the DC voltage change at point B (Figure 5) when the heating current is turned off. These pictures are then used to determine the quench speed. The AC circuits were operated at a frequency of 5000Hz so that the electronics will respond sufficiently rapidly to accurately depict the cooling curve of the specimen during a quench.

e. Calibration and evaluation

The AC circuits must be calibrated each time a different specimen is used. The calibration is done in the following manner: 1) the specimen is heated to some intermediate temperature determined by eye; 2) the specimen's resistance is measured with the DC circuits, and divided by its room temperature resistance to give the resistance ratio; 3) the AC current through the specimen is adjusted to make the digital voltmeter (or DC meter) read this ratio. After this calibration, the digital voltmeter (or DC meter) indicates the resistance ratio of the specimen to within a few tenths of a (or a few) per cent. The AC circuits make it relatively easy to get

the specimen to any desired temperature by minimizing the number of hunt and test operations necessary to obtain this temperature.

We intended to use this circuit in conjunction with other circuits to allow us to program the power supply to give slower quenches of any desired speed and shape. However, I found that slower quench speeds could be obtained quite satisfactorily by merely connecting a capacitor in parallel with the specimen and allowing the capacitor to discharge through the specimen, as discussed above. If capacitance discharge technique is not suitable for some future application, the programmed system could still be tried.

IV. TUNGSTEN QUENCHING RESULTS

A. Quench Speed Data

As stated in Section III C, the AC circuits are used in conjunction with an oscilloscope and Polaroid camera to determine quench speeds. In Figure 17 two of these pictures are drawn to scale. The vertical scale is proportional to the resistance of the specimen; since the resistance of tungsten is very nearly linear with temperature above room temperature, this scale is essentially proportional to the temperature of the specimen. The horizontal scale is proportional to time. A simplified fast quench speed picture, taken during a quench from 2905K, is shown at the top of the figure. The time scale is 20 milliseconds per division. The upper horizontal line is obtained by triggering the scope while the specimen is at the quench temperature; it marks this temperature on the vertical scale. The lower line is obtained by triggering the scope after the quench; it gives a base or zero temperature line. The curve between these lines gives the temperature of the specimen as a function of time during the quench. The quench speed is obtained by finding the slope of the first part of this curve as indicated by the dashed line in the figure. The first part of the curve is used because the vacancies are much more mobile at the higher temperatures, hence most of the vacancies lost during the quench are lost during this time. The fast quench speed calculations are accurate to about 10 per cent.

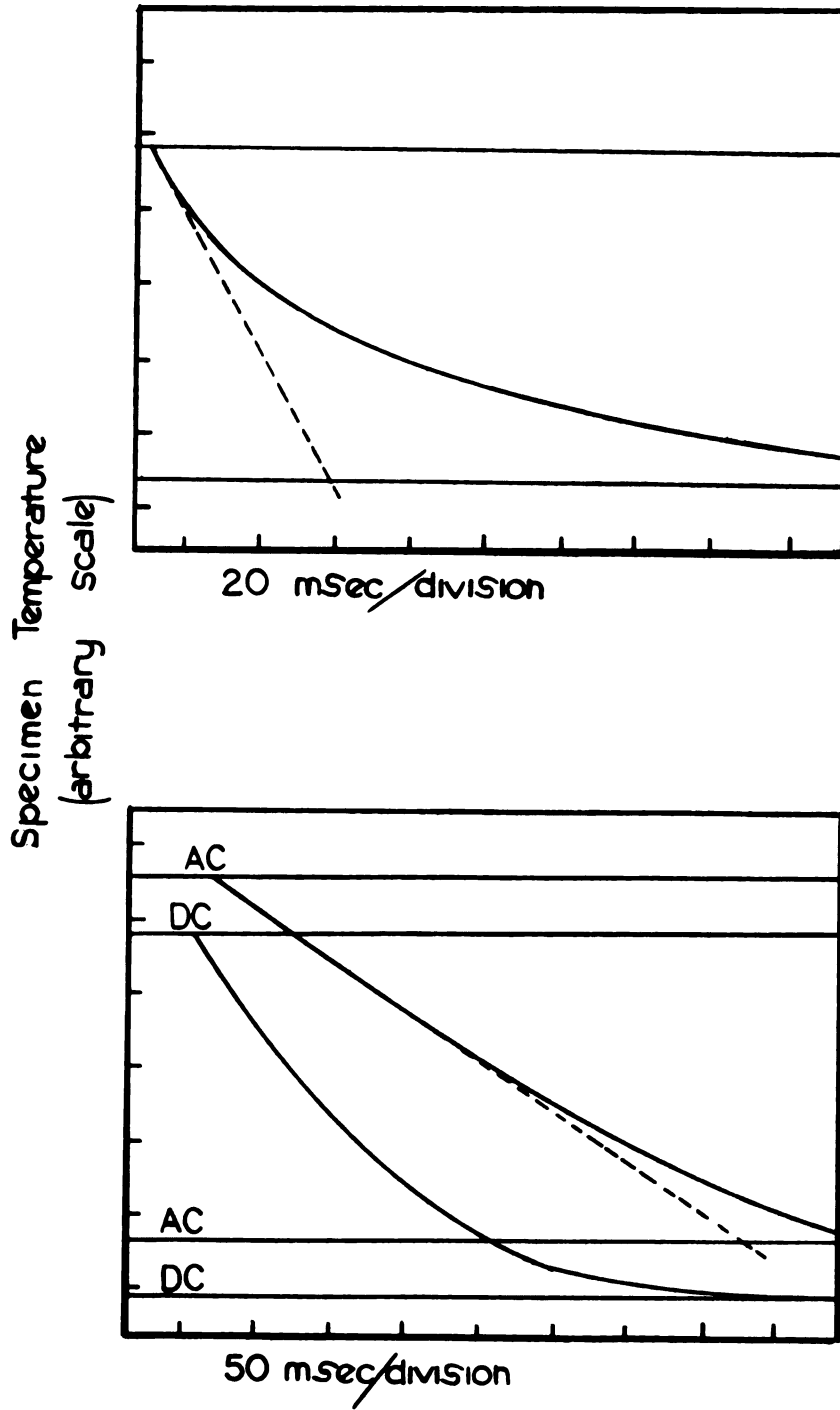


Figure 17: Quench Speed Graphs

A slower quench picture is shown at the bottom of the figure. This picture was taken during a quench from 2580K with an 1800 microfarad capacitor connected across the specimen to reduce the quench speed. The time scale was changed to 50 milliseconds per division. In this picture, the lines marked AC are equivalent to those in the upper picture. Here the slope is much easier to obtain because the curve is nearly linear; hence the slow quench speed determinations are accurate to a few per cent. The oscilloscope we use has a dual trace. The lines in the picture marked DC were obtained by using the second trace to monitor the DC voltage across the specimen. This gives a permanent check on the value of the capacitor used for a quench, since different capacitors discharge at different rates. For fast quench speeds there is no DC curve, of course, only an upper DC and lower DC line. These lines were left out of the upper picture.

Figure 18 illustrates how the quench speeds vary with quench temperature for a 1.2 mil specimen. Notice that the fast quench points have considerable scatter at high quench temperatures. This will be discussed later.

Figure 19 illustrates how the quench speeds vary with quench temperature for a 1.0 mil specimen. The fast quench speeds rapidly increase with increasing quench temperature, while the slower quench speeds are nearly independent of the quench temperature. Again most of the scatter is in the faster quench speeds. The small numbers by some of the points will be discussed later.

B. Fast Quench Tungsten Data

Figure 20 shows the fast quench speed data obtained for a 1.0 mil tungsten specimen. Here the quenched-in resistance is plotted on a

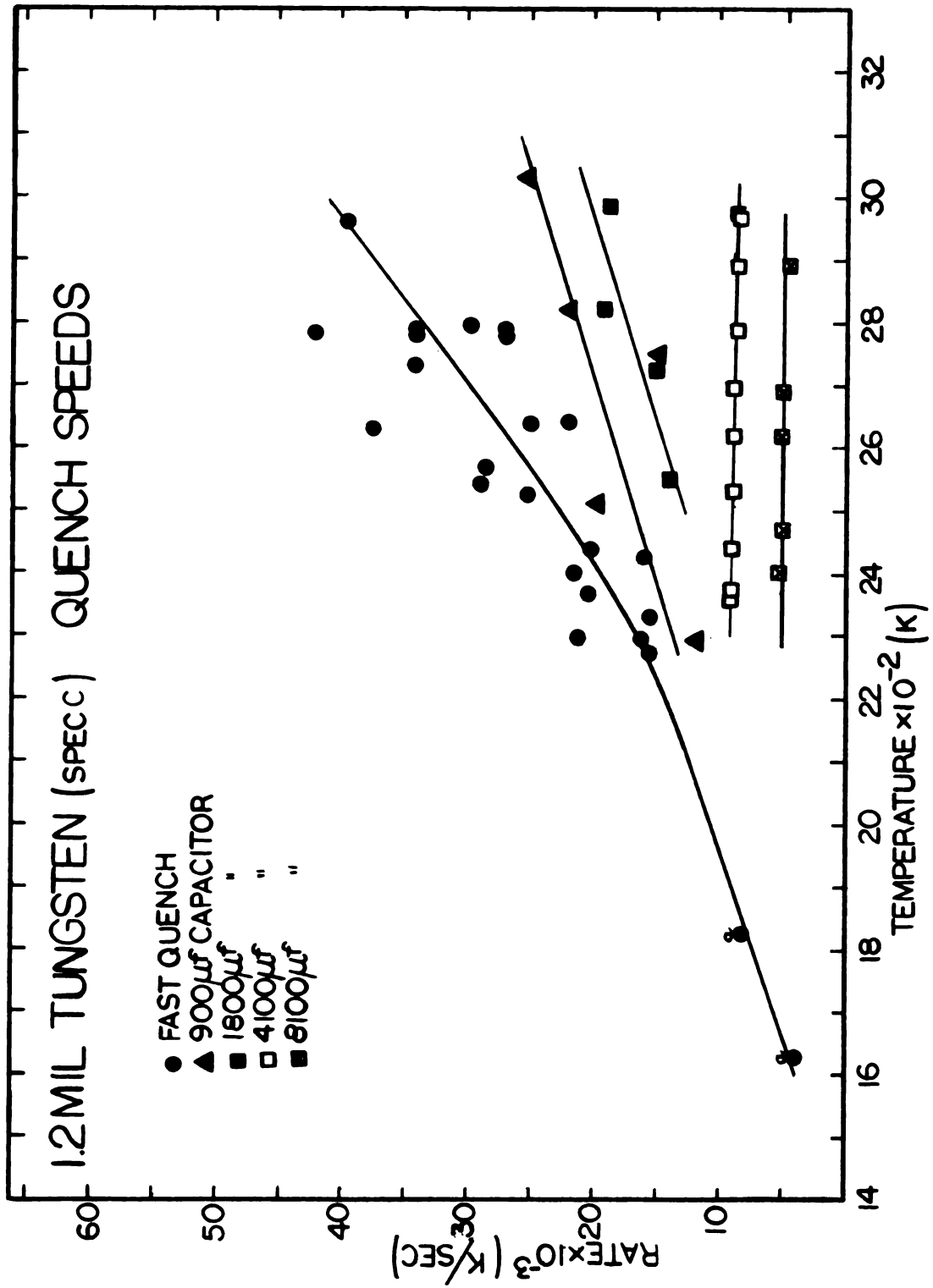


Figure 18: Quench Speed versus Quench Temperature for Specimen C (1.2mil)

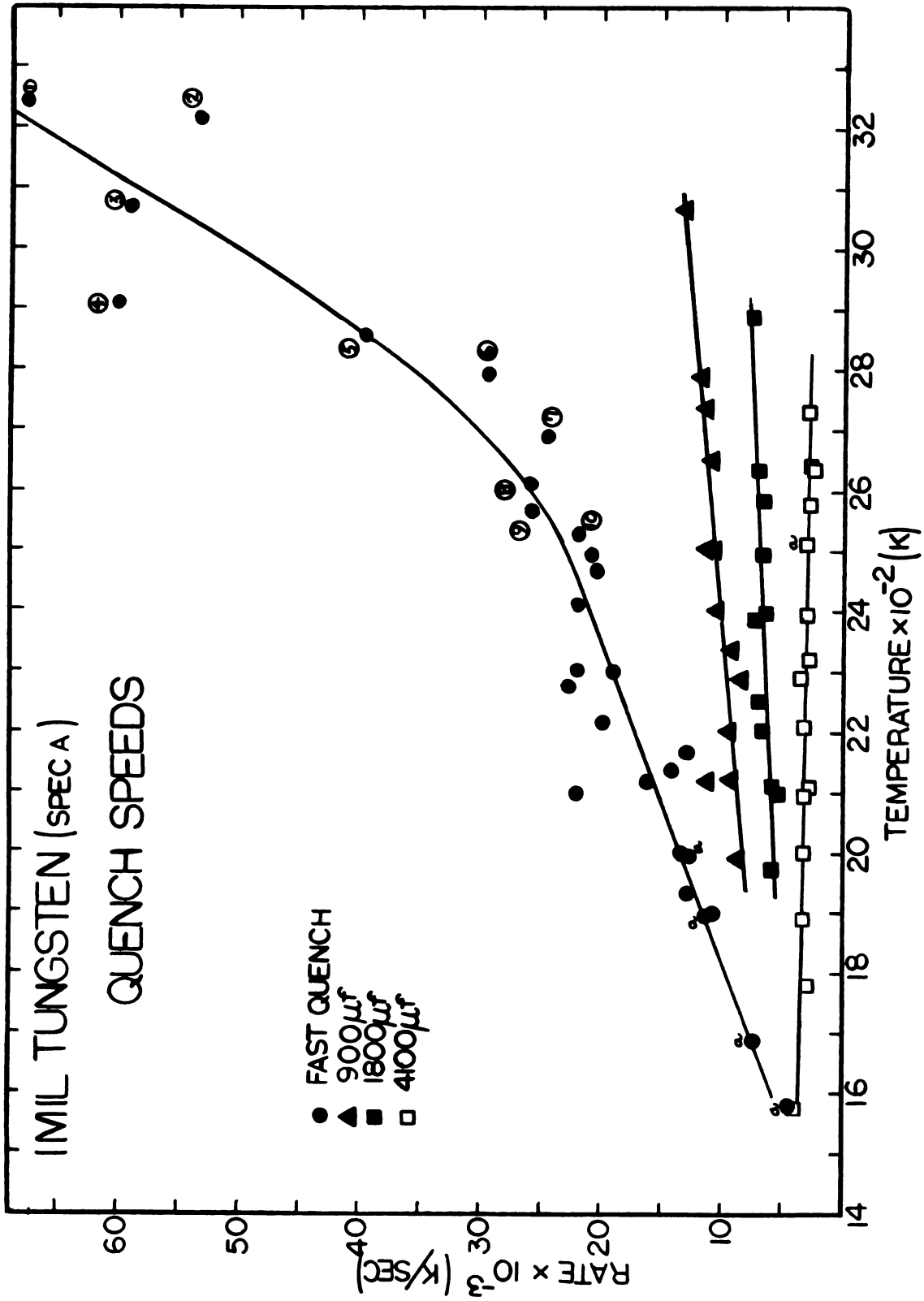


Figure 19: Quench Speed versus Quench Temperature for Specimen A (1.0mil)

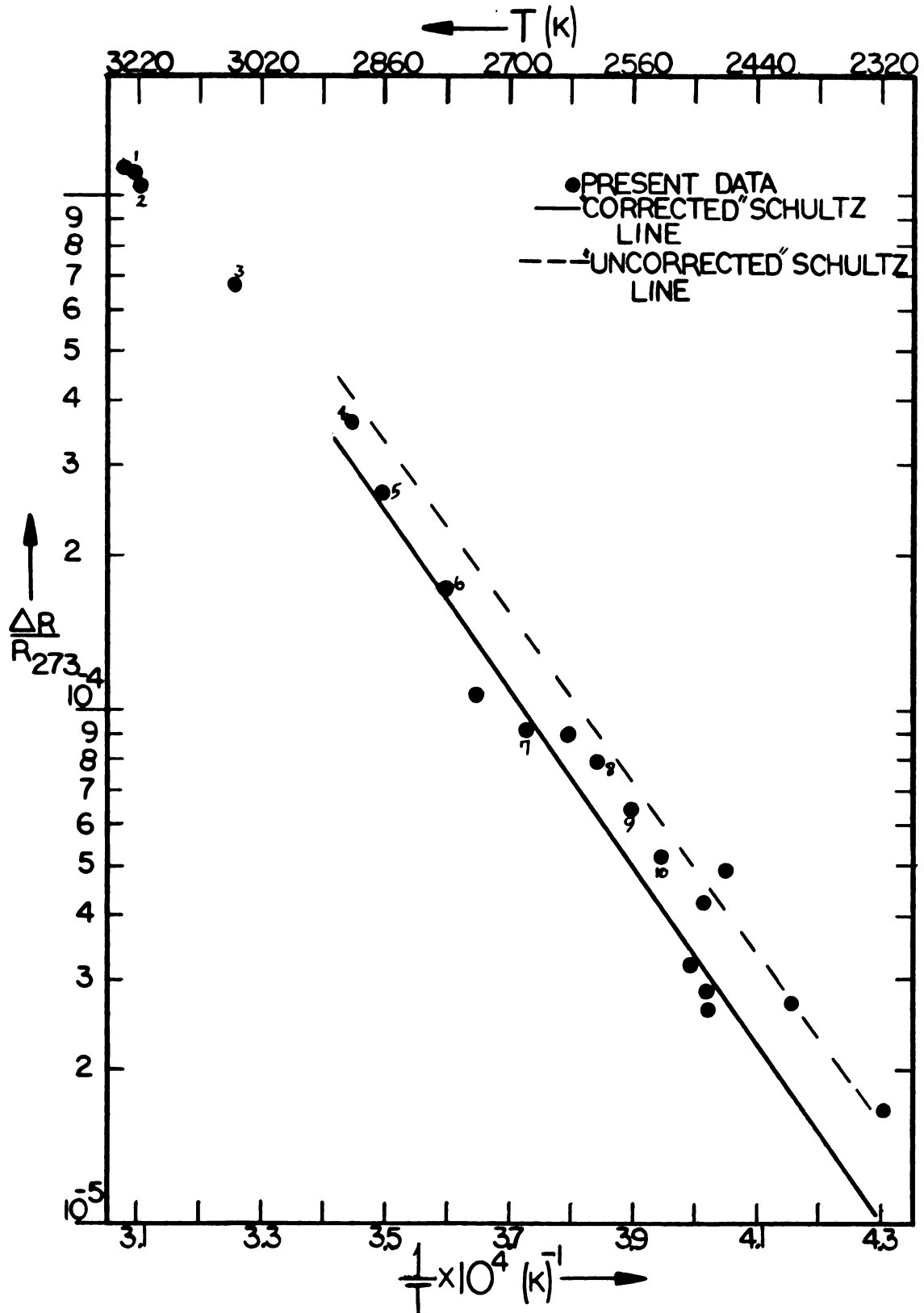


Figure 20: Fast Quench Data for Specimen A (1.0 mil)

logarithmic scale as a function of the inverse quench temperature. As stated above, the quenched-in resistance is divided by R_{273} to cancel the effect of the specimen geometry. From the equation for the equilibrium vacancy concentration (equation 1, page 1), this data should fall on a straight line with slope $-E_v^y/k$ if the quenched-in resistance is in fact proportional to the equilibrium vacancy concentration. The circles are our data and the solid line is a best fit line for Schultz's data (converted to $\Delta R/R_{273}$ and to our temperature scale). The dashed line is Schultz's data without the temperature correction.

Our data is in agreement with Schultz's data, except for the low quench temperature points. It is possible that this discrepancy arises from a small quenched-in resistance, apparently independent of the quench temperature, which should be subtracted from each of the data points to give the vacancy contribution to the quenched-in resistance. This will be shown and discussed in Figure 24. The correction does not affect the higher points because it is only a small fraction of the quenched-in resistance there.

The scatter at the low quench temperatures is due mostly to instability in the base resistance. At the higher quench temperatures, the scatter is probably due to variations in the quench speed. The small numbers by the high quench temperature points correspond to the numbers in Figure 19, the quench speeds for this data. There is good correlation between the quenched-in resistances and the quench speeds. When the quenched-in resistance is less than average, so is the quench speed, and vice versa. This correlation was found in all specimens. The origin of the quench speed scatter will be discussed in the next section.

Fast quench speed data obtained for two 1.2 mil and two 1.0 mil tungsten specimens are given in Figure 21. The solid circles are the data shown in Figure 19. The slopes are nearly the same for each set of data, so that they give nearly the same effective formation energy, $E_f^V = 3.1 \pm 0.2$ ev. However, the 1.2 mil data lie systematically above the 1.0 mil data. The most likely explanation for this shift is a systematic change in the temperature scales due to different resistance versus temperature curves for different specimens. A short paper published in 1962 by Davis,^{38/} indicates that errors of several hundred degrees are possible for tungsten wires which differ only in trace impurities. The data shifts more at lower temperatures than at higher temperatures as one would expect from a temperature shift. (Note in Figure 20 how Schultz's data changed for a constant temperature shift). If the data for the open circles are systematically shifted to the left by 110 degrees and the data for the closed circles shifted to the left by 70 degrees, they both coincide, to within the scatter of the data, with the 1.0 mil data.

Another possible, but less likely, explanation for the data shift is that different impurities, grain size, etc., cause different vacancy sink densities in different specimens. More or less vacancies would then be lost to sinks during the quench. This would result in different quenched-in resistances for different specimens.

C. Dependence of Quenched-in Resistance on Quench Speed

Figure 22 shows how the quenched-in resistance varies with quench speed for a 1.2 mil specimen (specimen C). The open circles and triangle were taken during the first run with this specimen. For some reason they

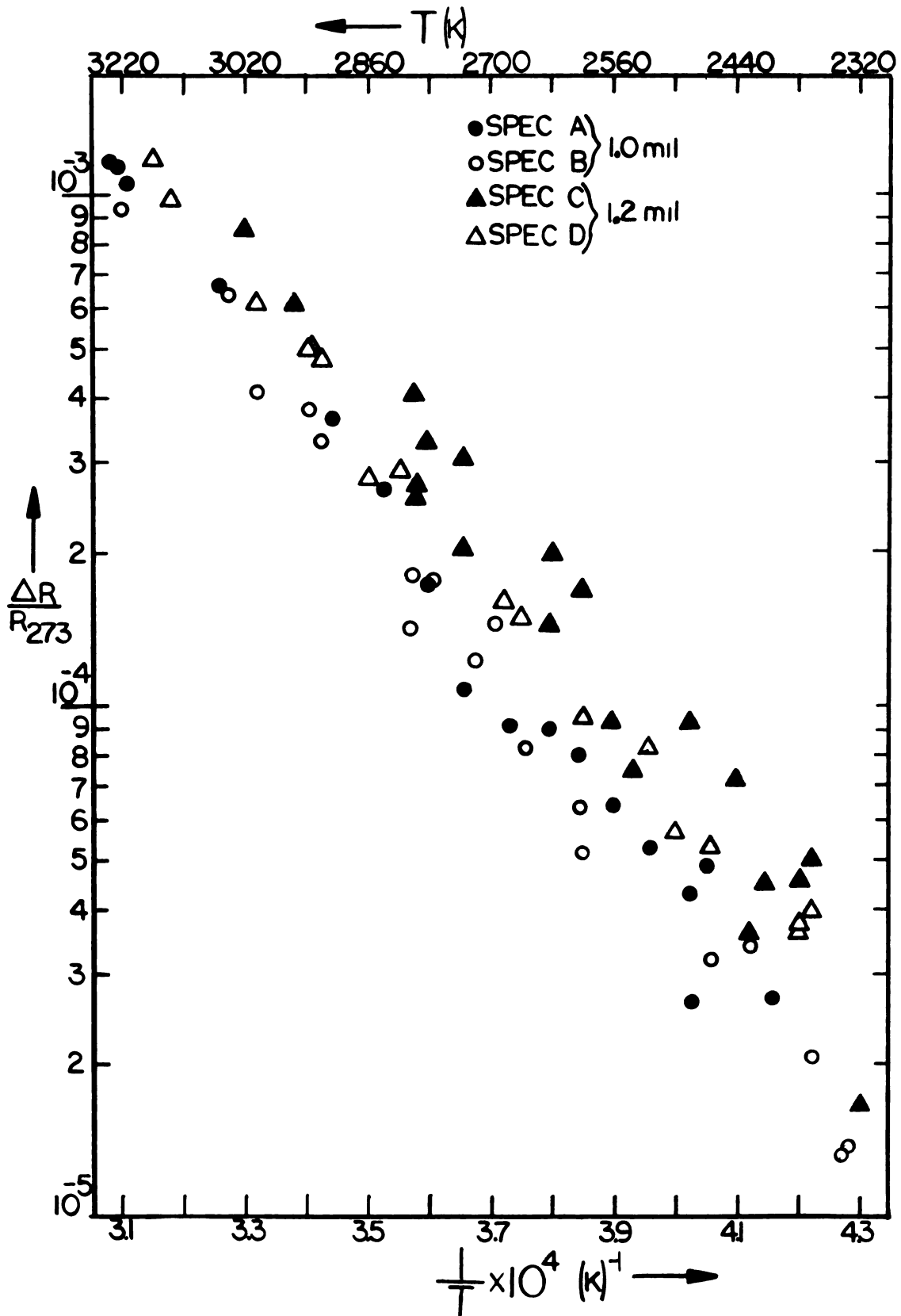


Figure 21: Fast Quench Data for Specimens A, B, C, and D

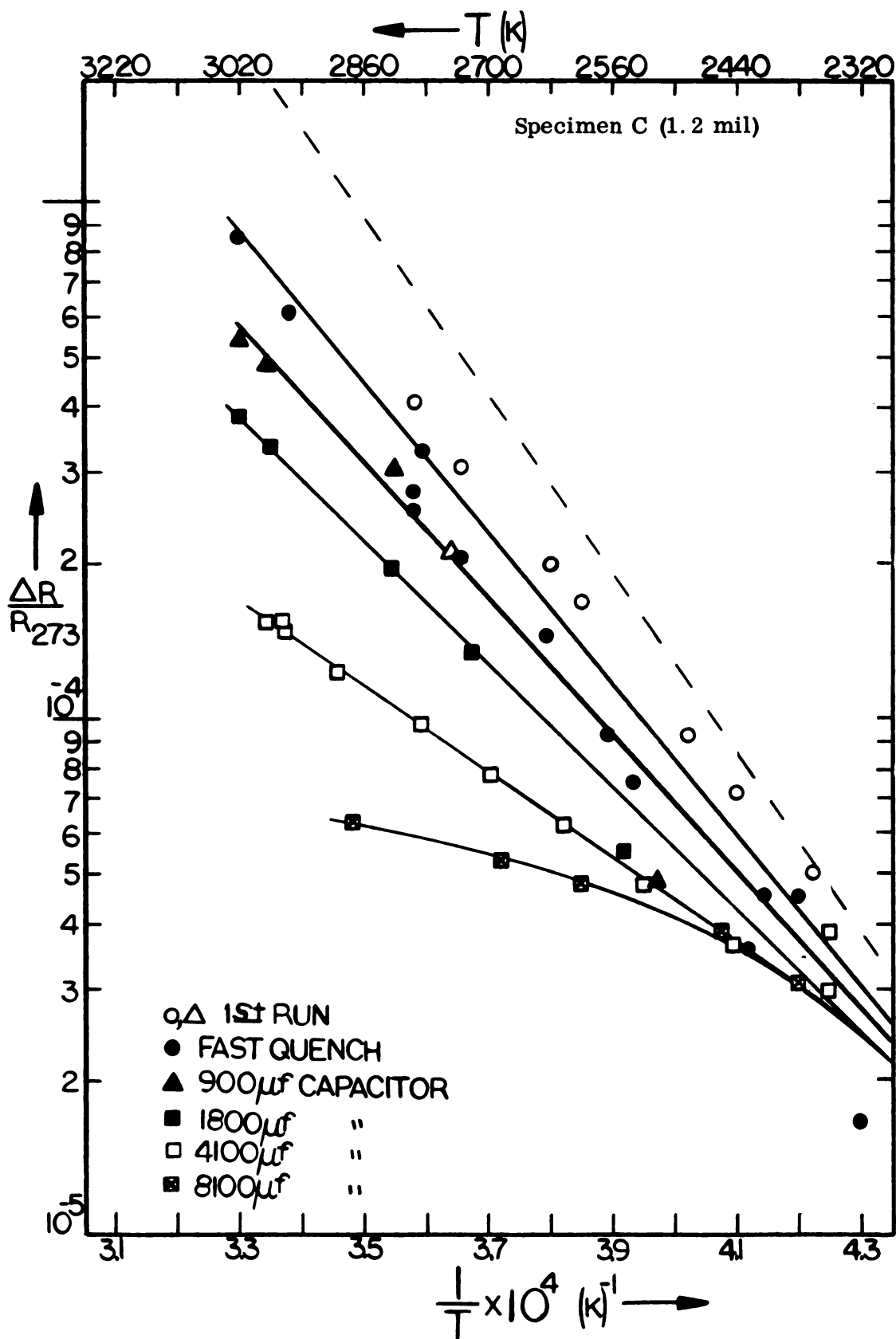


Figure 22: Dependence of Quenched-in Resistance on Quench Speed for Specimen C.

are systematically higher than the data taken on subsequent runs, hence they weren't considered when the fast quench speed line was drawn.

The circles are fast quench data with the quench speeds shown in Figure 18. The data for the triangles were obtained by connecting a 900 microfarad capacitor across the specimen to lower the quench speed. The other points were obtained by increasing the capacitance as shown, thereby lowering the quench speed. The dashed line in this figure and the next will be discussed in Section IV. F.

Figure 23 shows how the quenched-in resistance varies with quench speed for a 1.0 mil specimen (specimen B). These data show that the quenched-in resistance is dramatically affected by the quench speed. In later sections these data will be used to extrapolate to infinite quench speeds, and are compared to the predictions of Flynn's theory of vacancy annealing during a quench. Figure 24 shows similar data for another 1.0 mil specimen (specimen A). The quench speeds for this data are given in Figure 19. Data for a larger temperature range is shown here; the previous data all ended at an inverse quench temperature of 4.3×10^{-4} . This data shows that the quenched-in resistance does not continue to decrease with decreasing quench temperature as the vacancy concentration formula would indicate. Apparently for this specimen there is a small, temperature independent, contribution to the quenched-in resistance. We suspect that it is due to some impurity, probably carbon, being quenched into the lattice. ^{39/} The solubility of carbon in tungsten varies with temperature, reaching a maximum at about 2700K. ^{40/} When the specimen is slowly cooled to get a vacancy-free base, most of the carbon precipitates out of

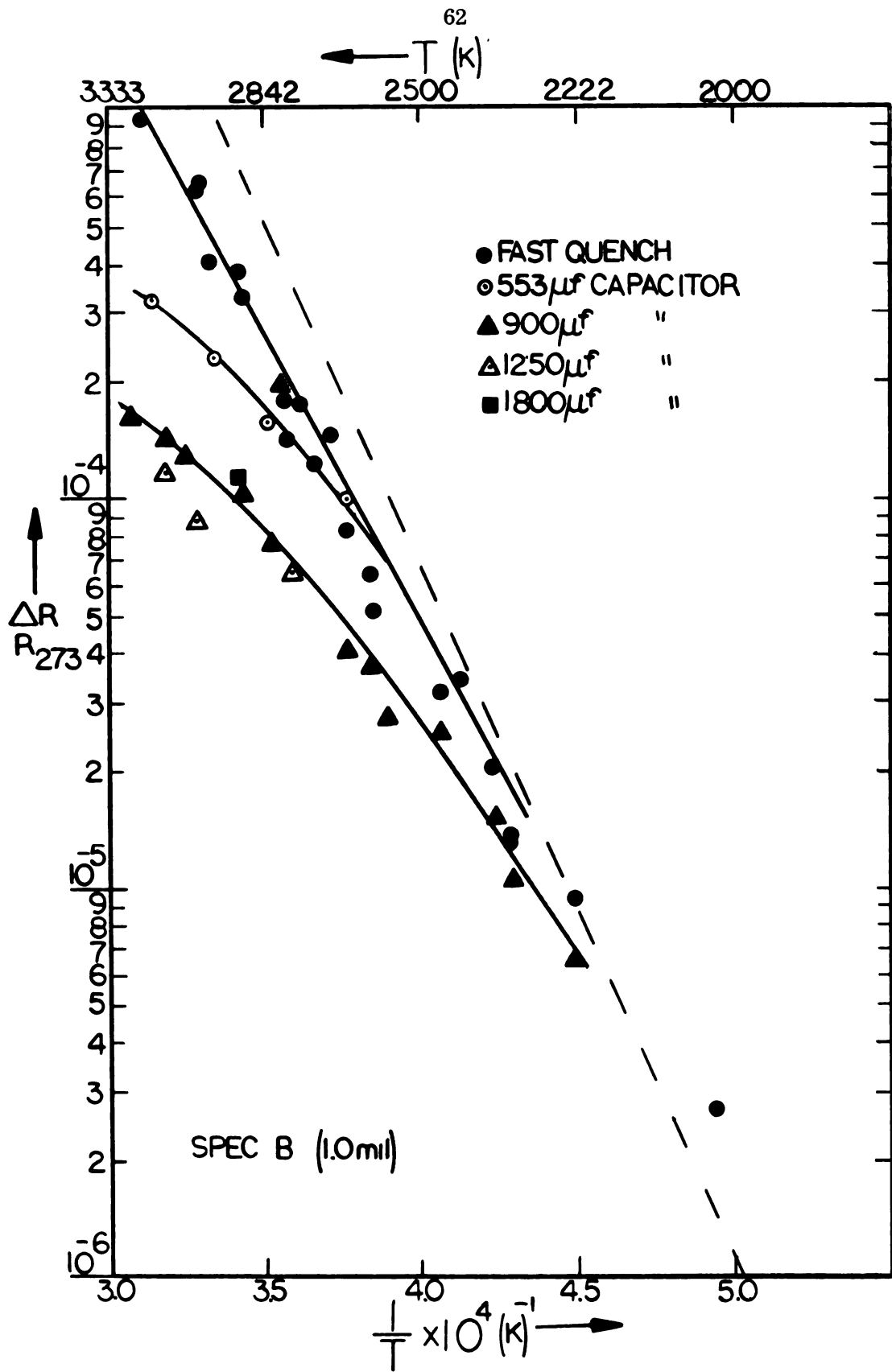


Figure 23: Dependence of Quenched-in Resistance on Quench Speed for Specimen B

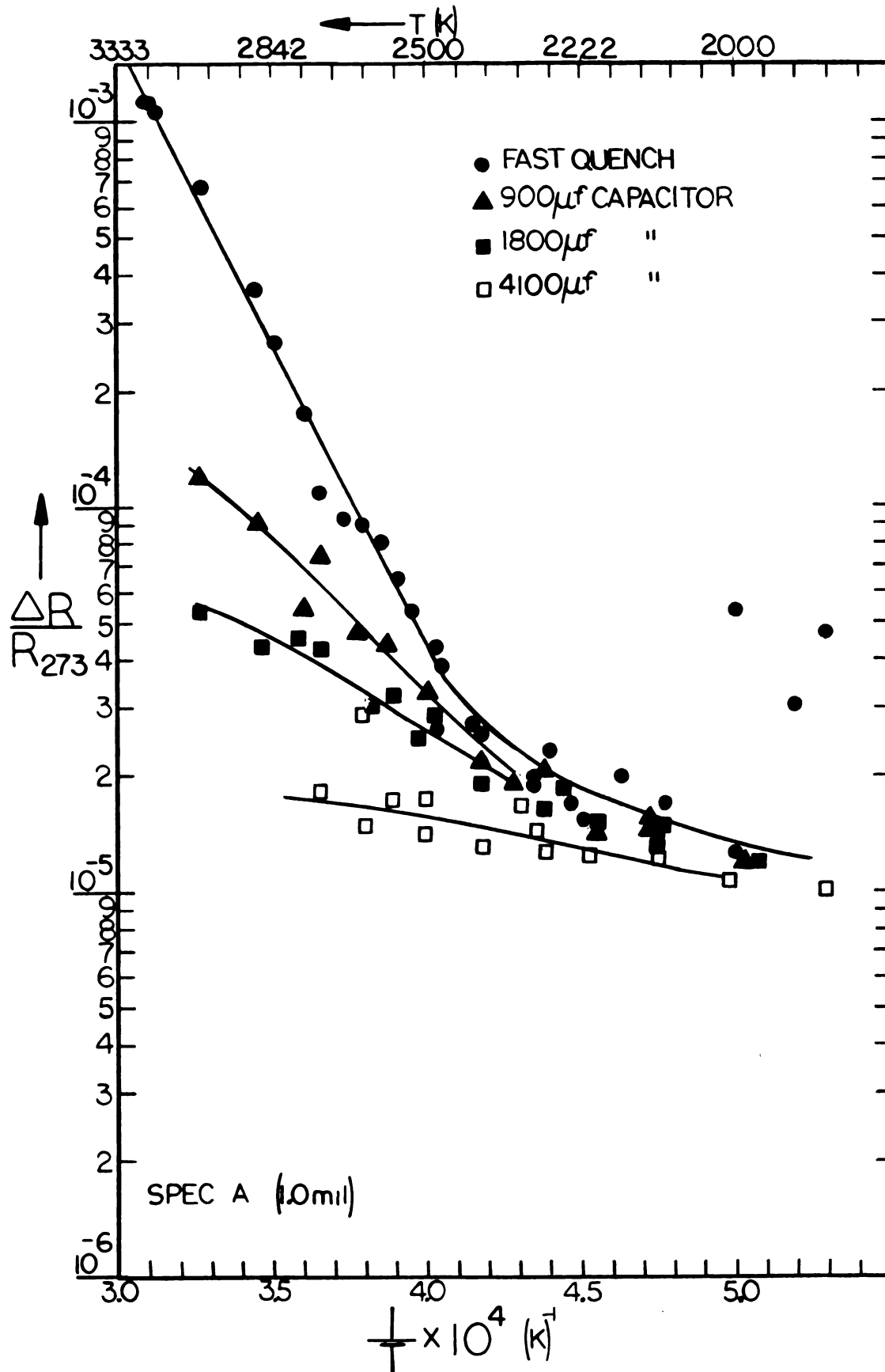


Figure 24: Dependence of Quenched-in Resistance on Quench Speed for Specimen A

the tungsten lattice to various sinks. However, during a quench the carbon is quenched into the lattice; it doesn't have time to leave the lattice before the temperature is too low for the carbon to move. This additional carbon in the lattice would increase the helium temperature resistance of the specimen. This is the quenched-in resistance which we propose to subtract from the data for specimen A shown in Figures 20 and 21. We do not have sufficient data to accurately determine the quenched-in resistance to be subtracted from the other specimens in Figure 21, but a few low temperature data points on each specimen indicate that the quenched-in resistance is considerably lower than for specimen A at the lower temperatures. The three high points in the lower right in Figure 24 are the first two points of one run and the first point of another run, taken before the base resistance had stabilized. This illustrates how critical the base resistance is for low temperature quenches. Figure 25 shows the data of Figure 24 with this constant quenched-in resistance subtracted from each data point. The data now decrease nicely into the next decade. The dashed line will be discussed in Section IV E.

D. Additional Tungsten Data

We have some fast quench data not shown in Figure 21. This data falls into four categories. First, we have data from high purity tungsten specimens which broke after a few quenches. This data is in general agreement with the data in Figure 21. Secondly, we have data from 2.0 mil tungsten specimens obtained from the Materials Research Corporation. This was their highest purity (99.999 per cent) tungsten. However, even

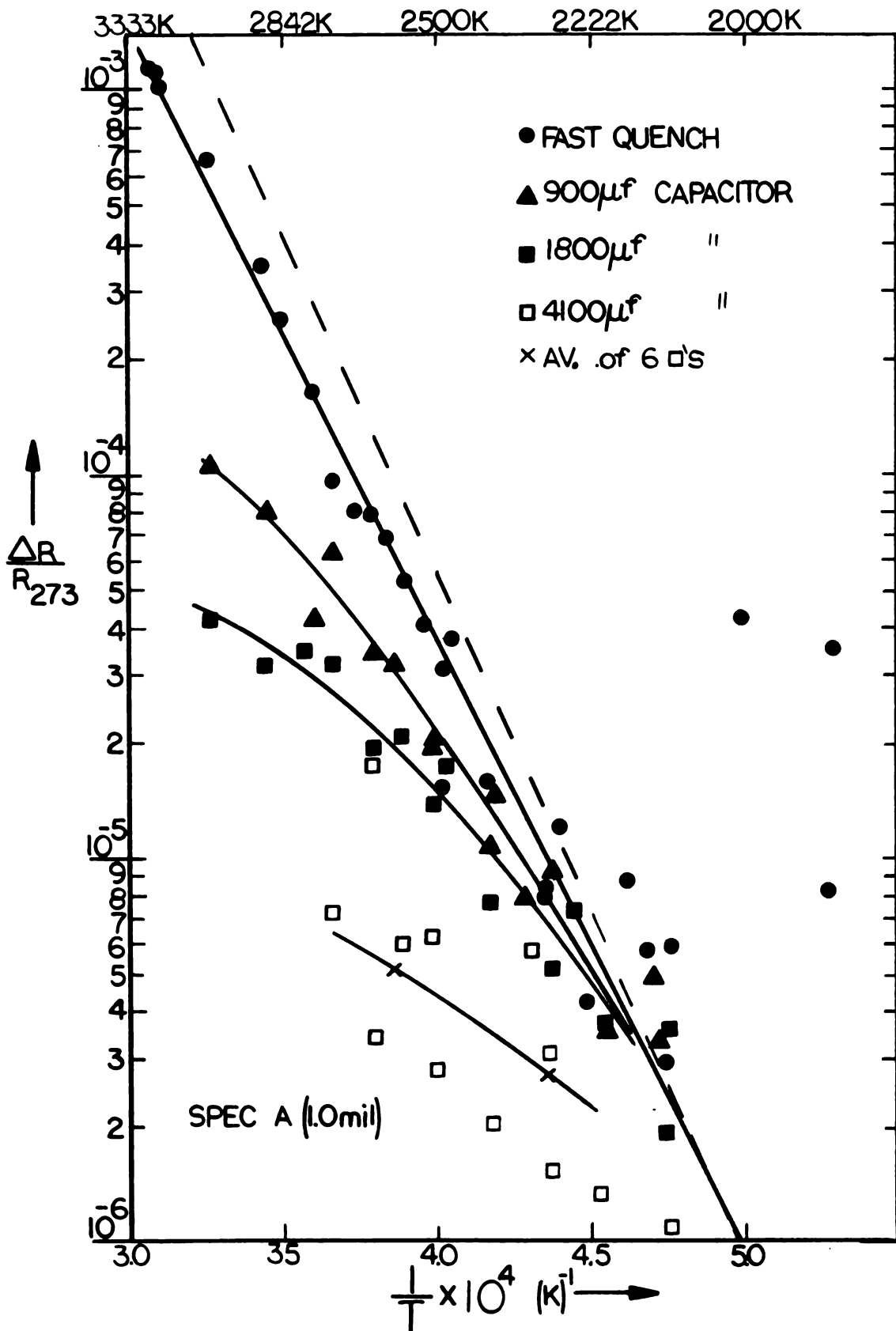


Figure 25: Dependence of Quenched-in Resistance on Quench Speed for Specimen A with constant subtracted

after extended annealing directly above superfluid helium we could not get the resistance ratio to rise above 400; with ratios of 250 more typical. This data has more scatter than that given above. The low temperature data was a factor of ten higher than that in Figure 21; while the high temperature data was only a factor of three higher. Thirdly, data on some Westinghouse HRE grade (lamp filament wire) tungsten were also obtained. After long anneals above the superfluid we obtained ratios of about 200. This data fell about a factor of two lower than the data in Figure 21, and again had substantial scatter. Fourthly, we have data on a very pure 2.0 mil tungsten specimen, kindly given to us by J.M.Galligan. This specimen was fabricated by carefully etching a high purity single crystal rod down to 2.0 mil diameter; it was not drawn. After being mounted on its holder, this specimen had an initial resistance ratio of 2670. A short series of anneals above the superfluid increased this ratio to over 5000. The data obtained from the first run with this specimen were in excellent agreement with the data from specimen A (1.0 mil). The data obtained from the second run were shifted upward by about 50K, in better agreement with the 1.2 mil data in Figure 21. The data from this very pure specimen confirms both the magnitude and the temperature dependence of our other data, and indicates that the shifts in the quenched-in resistance are present even in the purest specimens. These additional sets of data suggest that for purity less than that of our 600 ratio specimens, both the magnitude of the quenched-in resistance and effective formation energy are dependent on the purity of the specimen.

E. Experimental Accuracy of the Quench Data

The accuracy of the present quench data is limited by four factors: 1) uncertainties in temperature determination, already discussed on page 58; 2) carbon retained in solution as discussed on page 61; 3) changes in the base resistance, and 4) variations in the quench speeds. All other sources of error are insignificant compared to these four. We have checked two other possible sources of scatter. We found no difference in the quenched-in resistance for specimens annealed in hydrogen or helium. Also, there was no difference in the data when it was taken with ascending quench temperatures as opposed to descending quench temperatures.

The accuracy with which the specimen's temperature can be determined depends upon how accurately its room temperature and high temperature resistance can be measured, how constant its average temperature remains when it is hot, how uniform the temperature is along the specimen gauge length, and finally, how well its resistance ratio at a given temperature T , $R(T)/R_{273}$, corresponds to the value on the NBS temperature scale used to estimate its temperature. The specimen glows uniformly along the gauge length as far as the eye can tell. The room temperature and high temperature resistance can be measured with a precision of better than 0.1 per cent. Continuous readout on a digital voltmeter showed that short term fluctuations were less than 0.1 per cent of the high temperature resistance, and that long term variations occurred slowly enough so that they could be followed on the potentiometers. Taken together these three factors lead to an uncertainty in the specimen temperature of several degrees Kelvin. Therefore, the systematic difference in quenched-in resistance observed between 1.0 and 1.2 mil diameter specimens must be ascribed to differences

in the temperature scales, or to differing sink densities as discussed on page 58.

For low temperature quenches the quenched-in resistances are only a few per cent of the base resistance, hence, if the base resistance varies by as little as one per cent, large errors are introduced. To minimize this, the low temperature points were taken only after the base was stabilized as much as possible. If one is very careful, it is possible to keep the base fairly stable. For example, the base resistance changed only by 0.008 per cent during the measurements of the four lowest temperature points in Figure 24. These data were obtained after about fifty higher temperature points. When the base did change during a set of quench points, the base to which each quench point was referred was obtained by linearly interpolating between the initial and final bases, assuming that the base changed by the same amount for each quench.

After most of the data was taken, we formulated a possible explanation for much of the quench speed scatter. As stated above, the specimen cools primarily by radiation during the first part of the quench. For this reason, the temperature of the surroundings seen by the specimen is important. If the specimen were in a perfectly reflecting container, its surroundings would appear to be the same temperature as the specimen regardless of the temperature of the container walls; consequently, it would not cool at all by radiation. The dewar used for this experiment was nearly a "perfectly reflecting container"; it was silvered except for two 1-1/4 inch slits, and of course, the top of the dewar. The rate at which energy was radiated, therefore depended on the orientation of the specimen with respect to the slits in the dewar, and the depth of the spec-

imen in the dewar. When the specimen was perpendicular to the line of sight as viewed through the slits, it would see more room temperature than if it were rotated 90 degrees, in which case it would see mostly its own temperature reflected from the silvered walls.

To test this idea a few quenches were tried with 1.2 mil specimens in the two extreme orientations described above. The quench from the first orientation gave a higher quench speed than the second orientation (by about 10 per cent). To further test this idea, I built a "radiation shield" out of sheet metal covered with black friction tape. It went over the specimen as shown below.

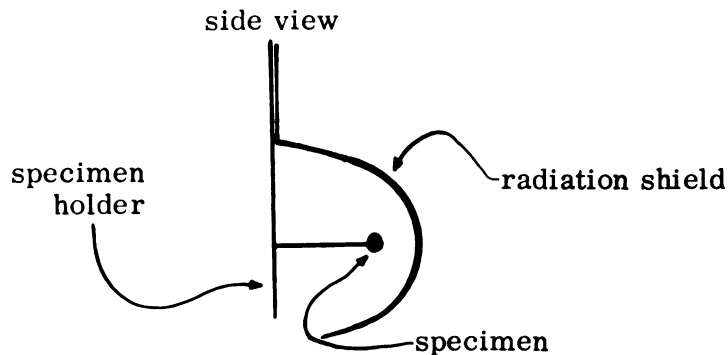


Figure 26: Radiation Shield

Several quenches were tried with the radiation shield in place. The results were inconclusive; a more detailed study will have to be made to determine if the radiation shield gives faster, more reproducible, quench speeds. With the radiation shield in place, the helium consumption was roughly twice as high for a given temperature, indicating that more heat was being absorbed in the helium rather than radiating out of the dewar.

F. Extrapolation

To estimate whether our fast quench speed was fast enough to quench in most of the equilibrium vacancy concentration, we extrapolated our data to infinite quench speed. For specimen A, quenched-in resistance values taken from smooth curves drawn through the data of Figure 25 were plotted on a logarithmic scale as a function of the inverse quench speed for a series of quench temperatures. ^{41,42,43/} The results are shown in Figure 27. Each curve corresponds to a different inverse quench temperature, as indicated. Each of the four quench speeds shown in Figure 25 contribute one of the four points for the constant quench temperature curves in Figure 27. The slowest quench speed data in Figure 25 give the points in the far right of Figure 27. These points are less critical than the others for the extrapolation, hence the large scatter of these points in Figure 25 has no significant effect on this extrapolation. French curves are used to carefully extrapolate these curves to zero inverse quench speed (infinite quench speed).

If this extrapolation is assumed to be valid* the quenched-in resistance corresponding to infinite quench speed can be read directly from this plot. The data along the line marked specimen A in Figure 28 show these quenched-in resistances plotted on a logarithmic scale as a function of the inverse quench temperature (same plot as the previous data). This data falls nicely on a straight line with an effective formation energy of 3.5 ± 0.2 eV. The error bars in Figure 28 represent the maximum possible errors in the quench speed and the quenched-in resistance. These possible errors introduce the ± 0.2 eV uncertainty.

*For a critical discussion of the validity of this technique see reference 43.

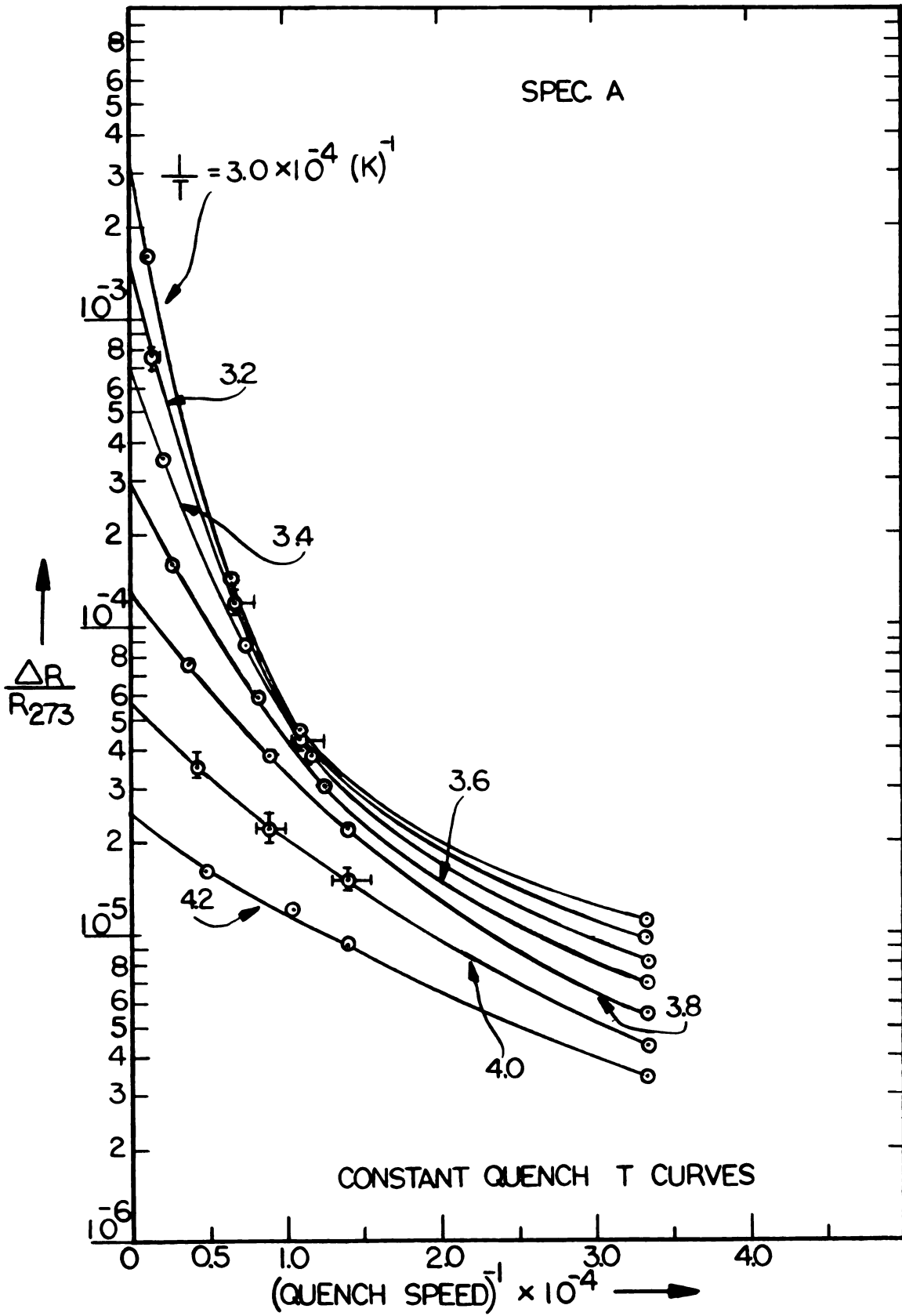


Figure 27: Data Extrapolation for Specimen A

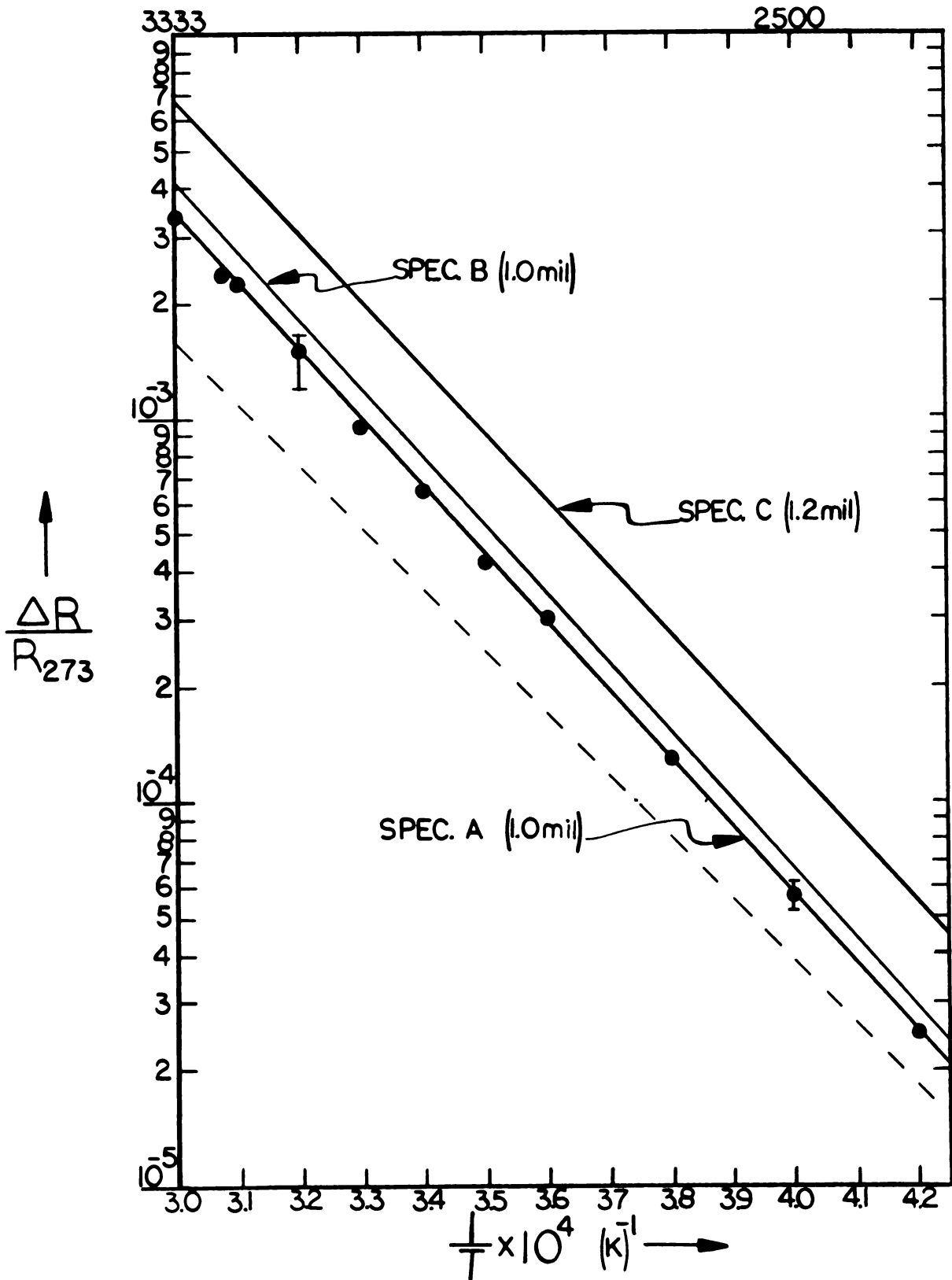


Figure 28: Extrapolated Infinite Quench Speed Data

The dashed line in this figure is a best fit line to the fast quench speed data for this specimen.

A similar analysis was also performed on specimen B (1.0 mil) and on specimen C (1.2 mil). Both of these specimens give extrapolation curves similar to these shown in Figure 27. The lines marked specimen B and specimen C in Figure 28 are best fit lines to the infinite quench speeds for those specimens. As in Figure 21, the 1.2 mil data lies above the 1.0 mil data, but they both give an infinite quench speed effective formation energy of 3.5 ev. Again there is an uncertainty of about ± 0.2 ev associated with possible errors in the quench speed and quenched-in resistance values. We did not get enough low quench speed data on specimen D to perform this analysis on it.

G. Flynn Theory Analysis

We have also attempted to compare our data with the predictions of Flynn's theory^{44/} of vacancy annealing during a quench. This theory assumes that the concentration of single vacancies is changed during the quench only by annihilation of vacancies at fixed sinks (eg. grain boundaries and dislocations). For quenches in which the temperature decreases linearly with time, the fraction of vacancies lost during a quench is shown to depend, to good approximation, only on the product $D_q T_q \mathcal{T}_q$, where D_q is the vacancy diffusion coefficient at the quench temperature T_q , and \mathcal{T}_q is the quench time. For the slower quench speeds the temperature of the specimen decreases nearly linearly with time as shown in Section IV A. For the fast quench speeds the temperature does not decrease linearly with time; but in the high temperature region where one expects most of the

vacancies to be lost, a linear approximation is not too bad; this is in fact the way the quench speeds were calculated.

For a given fractional vacancy loss during the quench, eg., 50 per cent, the theory leads to the equation,

$$D_q T_q \tau_q = Z,$$

where Z is a constant. Since D_q is proportional to $\exp(-E_m^v/kT)$, the relation

$$D_o^v \exp(-E_m^v/kT_q) = Z/T_q \tau_q$$

follows. To test this theory, $\ln(1/T_q \tau_q)$ is plotted against $1/T_q$; if the data is consistent with the theory, a straight line will result.

The data in Figures 22, 23, and 25 were used to test the theory. The dashed lines in Figures 22, 23, and 25 are the infinite quench speed lines obtained in Figure 29. Two separate tests of the theory were made. First, the fast quench speed data were assumed to represent infinite quench speed for the Flynn analysis. The upper half of Figure 29 shows plots of $\ln(1/T_q \tau_q)$ versus $1/T_q$ resulting from this assumption, for all three sets of data. The error bars represent possible errors in the quench speed determinations. These results have considerable scatter, but if a "best fit" slope is determined, one obtains a vacancy motion energy of 1.1 ± 0.4 eV.

If the fast quench speed effective formation energy is added to this vacancy motion energy, one obtains a value of 4.4 eV for Q . This value is considerably lower than the lowest Q listed in Table 1 (5.2 eV).

The second test of Flynn's theory was made by using the extrapolated data in Figure 28 as the infinite quench speed data. The lower half of Figure 29 shows plots of $\ln(1/T_q \tau_q)$ versus $1/T_q$ for this data, again for

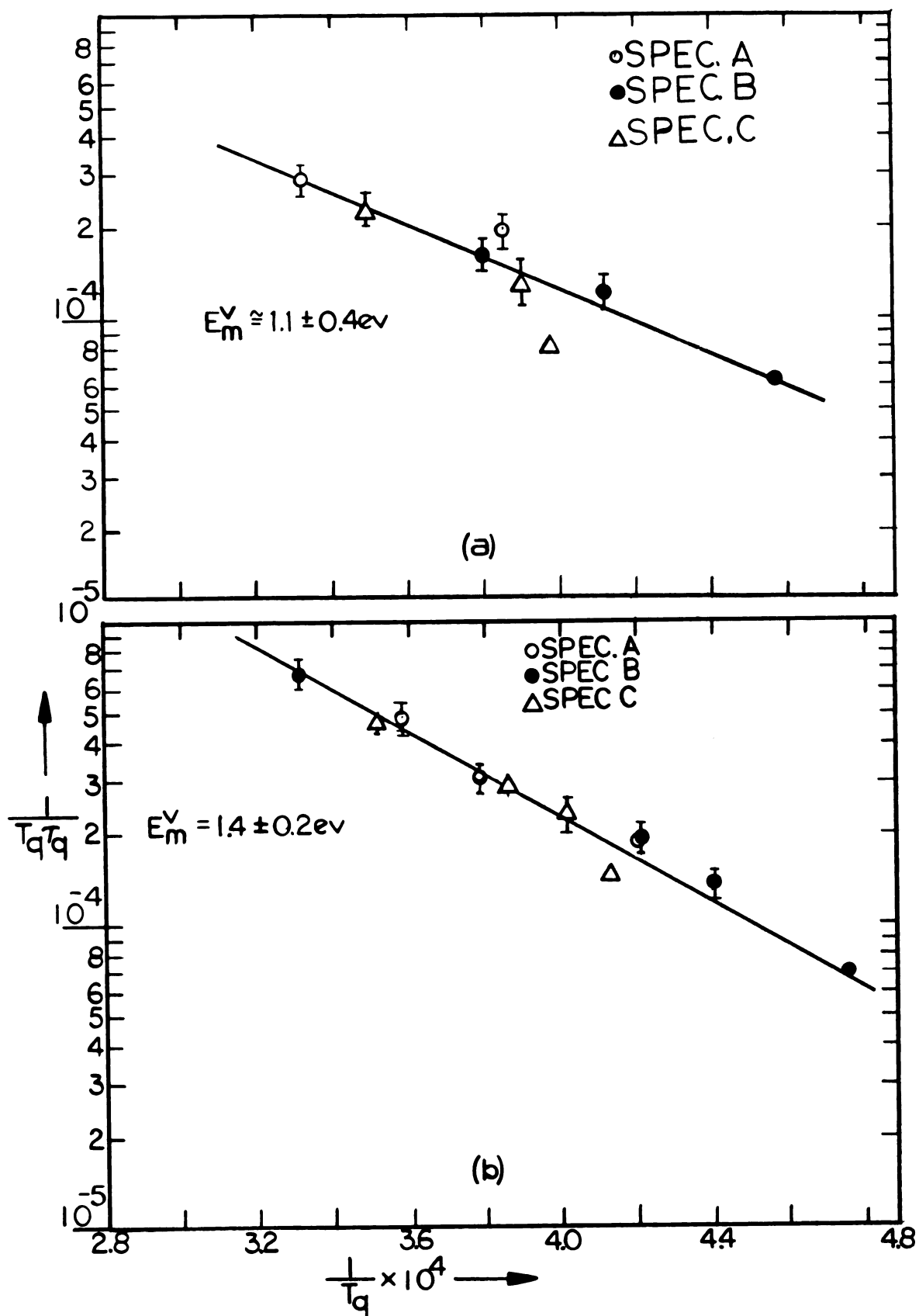


Figure 29: $1/T_q \tau_q$ versus $1/T_q$ Plots for the Flynn Analysis

all three specimens. There are three additional points on this graph because the fast quench speed data is now included. These results fall nearly on a straight line, allowing the slope to be determined more precisely than above. This data yields a vacancy motion energy of 1.4 ± 0.2 ev. If the effective formation and motion energies (3.5 ± 0.2 and 1.4 ± 0.2 ev) used for this analysis are added together, a value of 4.9 ± 0.4 ev results for Q . This is consistent with the 5.2 ev value in Table 1, but considerably lower than the 5.89 ev and 6.6 ev values.

We conclude that our data appear to be generally consistent with Flynn's theory, but that scatter in the data, and the lack of a clearly established value for Q make a positive conclusion unwarranted at this time. If our upper limit of $E_f^V = 3.7$ ev is used in the Flynn analysis, a vacancy motion energy of 1.9 ± 0.6 ev results. Hence, if the Flynn theory is valid, it would be difficult to reconcile our data with a value of Q much over 6.0 ev.

V. ANNEALING OF DEFECTS QUENCHED INTO TUNGSTEN

In addition to measurements of the quenched-in resistance, some studies were also made of the annealing out of this resistance in order to obtain information about the mobility of the quenched-in defects. For these studies the specimen was first quenched in the superfluid as described above, and the quenched-in resistance measured at the superfluid temperature. The helium pump was then turned off and helium gas bled into the dewar until the pressure was up to atmospheric pressure. This was done because it was much easier to get the specimen in and out of the dewar at atmospheric pressure, and because much less liquid helium was used when the experiment was done at 4.2K. The helium temperature resistance was then re-measured, with the specimen about an inch below the liquid surface where the liquid should have been warmed to nearly 4.2K by the warm helium gas bled in. This was done to obtain a 4.2K resistance reading, because all of the annealing data was taken at this temperature. The change in resistance between 1.3 and 4.2K was small, typically less than one per cent of the quenched-in resistance. The specimen was then removed from the cryostat and placed in the NRC evaporator, which was evacuated to less than 2×10^{-5} Torr. In this vacuum the specimen was resistance-heated to the annealing temperatures. After the specimen was heated to the annealing temperature, its resistance (hence temperature) was held constant to within a few tenths of a per cent.

A. Isochronal Anneals

We first performed isochronal anneals to find the temperature range in which the quenched-in resistance anneals away. An isochronal anneal consists in heating the specimen for a fixed time (eg. 5 minutes) at a series of increasing temperatures until most of the quenched-in resistance anneals away. Figure 30 shows data obtained from four isochronal anneals on two different specimens quenched from temperatures in the 2800 to 3000K range. Here the fraction of the quenched-in resistance remaining is plotted as a function of the annealing temperature. The solid circles and squares are data obtained from the first run on each specimen; the open circles and squares are from the second run on each specimen. These data were taken using five minute holding times. There are three regions in the recovery: 1) the low temperature region; 2) the major recovery stage in the vicinity of 950K, and 3) the high temperature region above the recovery stage.

The resistance of the specimen always increased when it was cycled from 4.2K to room temperature and back. However, the resistance usually returned to the original quenched resistance after the specimens were taken out of the cryostat and allowed to warm in the room. In all cases the resistance went back to the original quenched resistance after the first resistance-heated anneal (650-850). In addition, tests showed that for a given specimen this increase in resistance upon cycling from 4.2K to room temperature and back was very nearly the same whether the specimen had been quenched or not. For these reasons, we do not believe that this resistance increase is likely to be associated with vacancies. Rather, we are inclined to attribute it to a surface impurity effect.

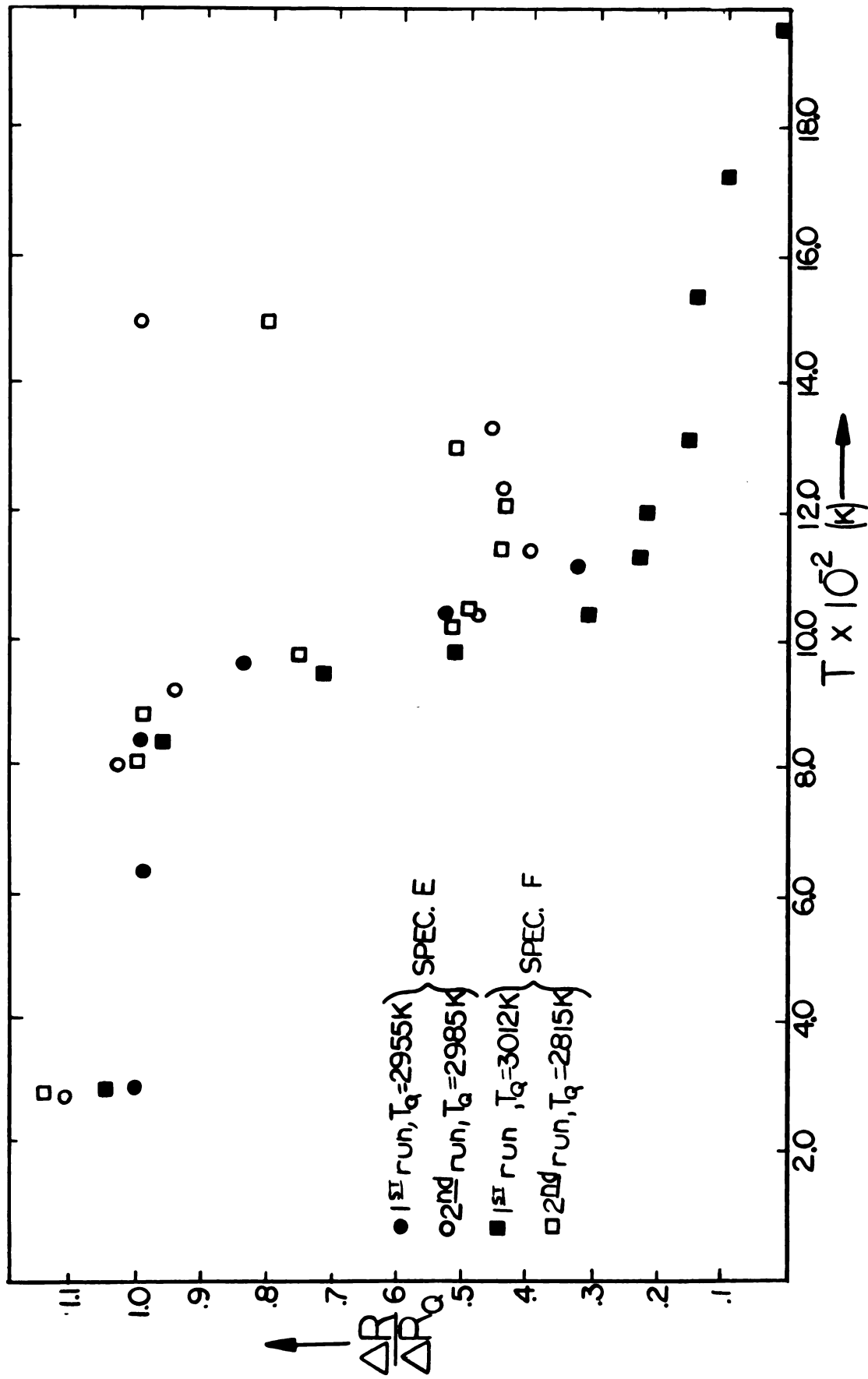


Figure 30: Isochronal Anneals for Specimens Quenched from 2800 to 3000K

The major recovery stage at about 950K, in which over half of the quenched-in resistance anneals away, occurred in each run for each specimen. The data indicated by the solid squares decreased until only a small fraction of the original quenched-in resistance was left, as one would expect when simple defects are annealing away. The data for the solid circles behaved similarly, but terminated abruptly because the specimen broke. The open circles and squares, the second run for both specimens (the solid circle specimen was spot-welded together outside the new gauge length), begin to increase after reaching a minimum of about 45 per cent. After the resistance of these specimens increased, we tried some quenches from 2000K to 2500K. The quenched-in resistances were one hundred times higher than the "normal" quenched-in resistances. This strongly suggests an impurity problem. After a high temperature (above 2700K) quench or anneal, further quenching gave "normal" quenched-in resistances, showing that this anomaly can be removed.

Note that the quench temperatures are in the 2800 to 3000K range. Since the solubility of carbon in tungsten reaches a maximum at about $\frac{40}{2700}$, quite near the quench temperature, we suspect these increases are caused by carbon redistributing itself in the lattice. To test this hypothesis we performed two more isochronal anneals on a specimen which had been quenched from over 3200K. At this temperature the carbon solubility decreases by a factor of three from its value at 2800K.

The results are shown in Figure 31. The holding time was increased to ten minutes so that the time taken to get to the annealing temperature was a smaller fraction of the total annealing time, allowing more precise data to be obtained. The solid circles represent the first run and the open

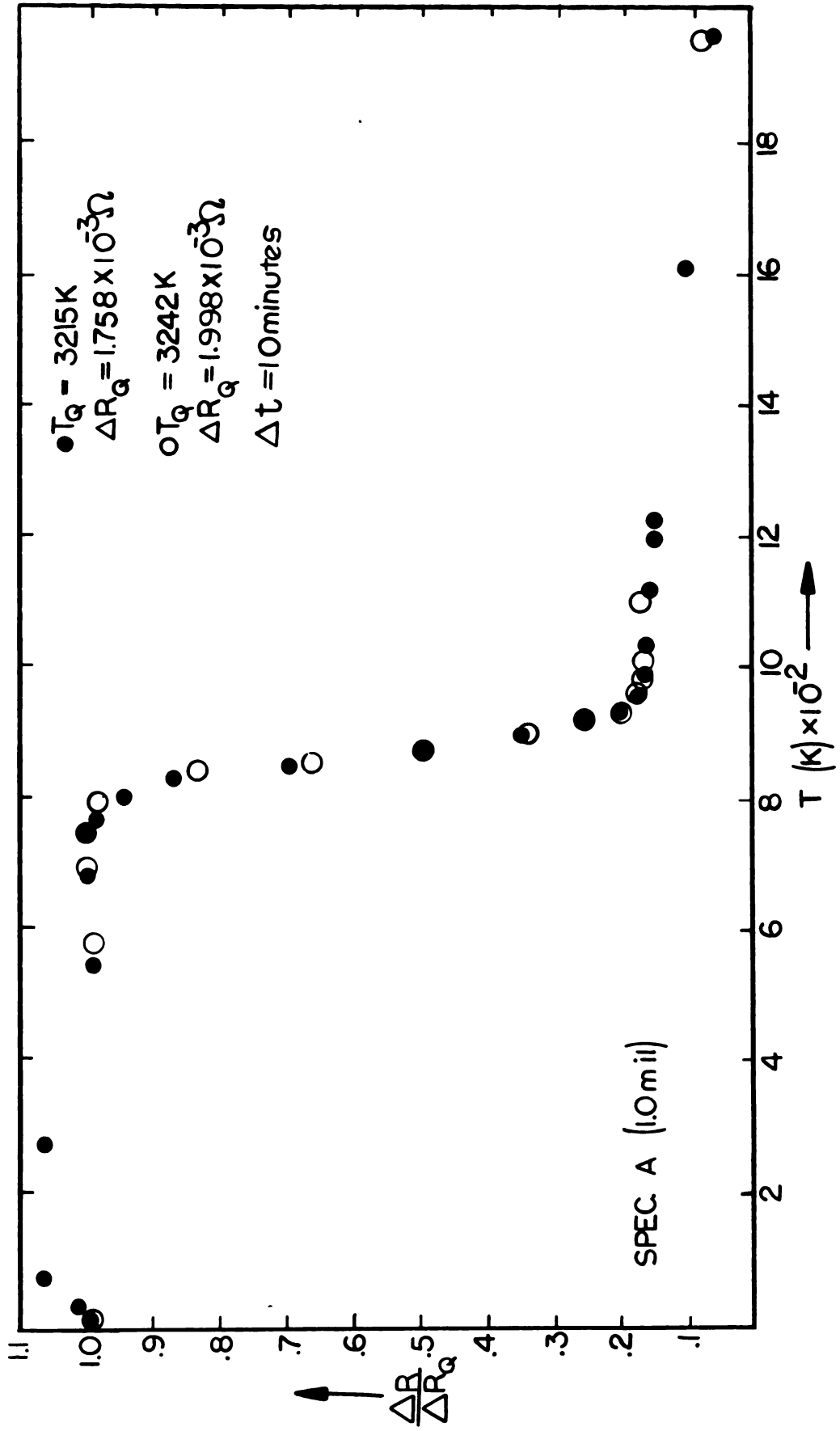


Figure 31: Isochronal Anneals for Specimen A Quenched from Temperatures above 3200K

circles the second run. In both runs the quenched-in resistance decreases to a small fraction of the original quenched-in resistance. This time the data are very reproducible from one run to the next. The recovery stage is now centered about 850K, approximately 100 degrees lower than for the specimens quenched from 2800 to 3000K.

We conclude that most of the resistance quenched into tungsten anneals away in a single, sharp recovery stage in the range of 800-1000K. This is in agreement with Stage IV recovery in radiation damage studies which Galligan et. al. ^{4,20/} showed to be due to vacancy migration.

We have analyzed the data of Figure 31 using the chemical rate equation ^{18,20,45/} frequently used in radiation damage studies. We do not propose to justify this analysis; it is used only to compare the motion energy obtained from our data to those calculated from radiation damage studies. The chemical rate equation ^{45/} can be written as:

$$\frac{d\rho}{dt} = -\nu\rho^{\gamma}\exp(-E_m^v/kT) \quad (4)$$

where ρ is the quenched-in resistivity, t is time, ν is the frequency factor, γ is the order of the reaction. This is the same as equation (3a) except that $F(\rho)$ is assumed to be $\nu\rho^{\gamma}$. For an isochronal anneal, T is constant during a given heat pulse allowing (4) to be integrated directly. For a first order process $\gamma = 1$ and (4) integrates to

$$\ln(\rho_i/\rho_f) = \nu T \exp(-E_m^v/kT). \quad (5)$$

For a second order process, $\gamma = 2$ and (4) integrates to

$$\rho_f^{-1} - \rho_i^{-1} = \nu T \exp(-E_m^v/kT). \quad (6)$$

Here ρ_i is the vacancy resistivity at the beginning of the jth heating pulse at temperature T_j , ρ_f is the vacancy resistivity at the end of this pulse; \mathcal{T} is the pulse time. If ρ_i is assumed to be proportional to ΔR_i , the vacancy resistance (i. e., $\rho_i = K\Delta R_i$), then equations (5) and (6) can be written as

$$\ln \left[\frac{\Delta R_i}{\Delta R_f} \right] = \nu \mathcal{T} \exp \left[\frac{-E_m^v}{kT} \right] \quad (7)$$

$$(\Delta R_f)^{-1} - (\Delta R_i)^{-1} = K\nu \mathcal{T} \exp \left[\frac{-E_m^v}{kT} \right] \quad (8)$$

respectively. To test for a first order process, $\ln \left[\ln \left(\frac{\Delta R_i}{\Delta R_f} \right) \right]$ is plotted against $\frac{1}{T}$ and the resulting plot examined for linearity. Similarly, to test for a second order process, $\ln \left[(\Delta R_f)^{-1} - (\Delta R_i)^{-1} \right]$ is plotted against $\frac{1}{T}$. We have performed both of these tests on the major recovery stage in Figure 31 using the end of the major stage as the base. The first order test gives linear results only over one decade for the temperature range 785K to 855K. If an effective motion energy is calculated, a value in the range of 2.2 ev results. The second order test shown in Figure 32 gives nearly linear results in over three decades, covering the temperature range 785K to 950K. This analysis gives an effective motion energy of about 2.5 ev. These effective motion energies lie about midway between the estimates of 1.7 ev and 3.1 ev obtained from radiation damage and cold work studies for Stage III and Stage IV respectively. As we will discuss below, isothermal anneals after quenches from about 3200K yield data which cannot be adequately described by equation (4). We therefore tend to believe that this second order fit is at least partly accidental, and that the effective motion energy obtained must be treated with extreme caution.

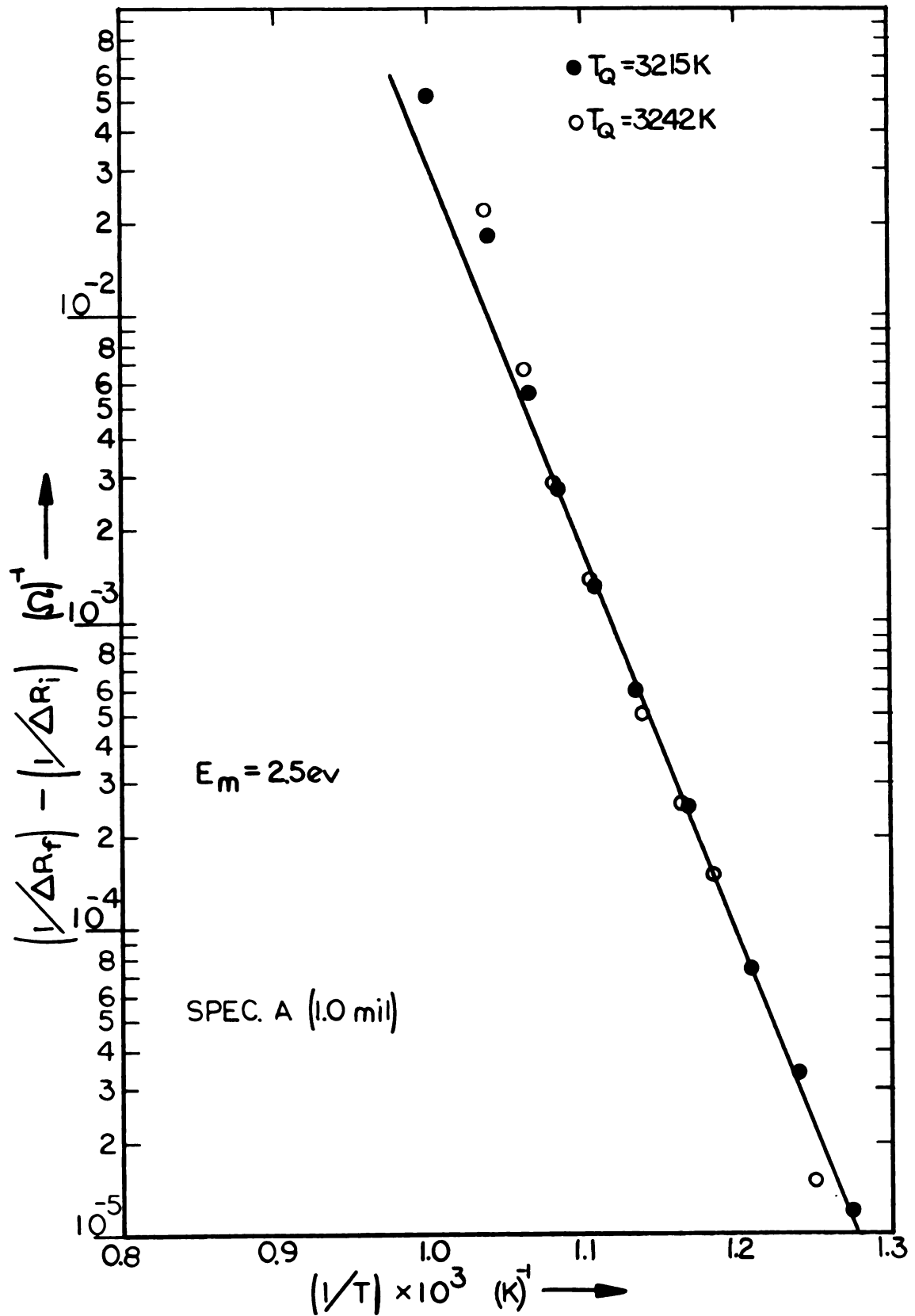


Figure 32: Second Order Analysis of the Data from Figure 31

The data are not consistent with the "first order" kinetics reported by Galligan^{20/} for Stage IV recovery in radiation damaged tungsten. Either the process by which vacancies are annihilated is different in radiation damaged specimens than in quenched ones, or one of these analyses obtain agreement with simple kinetics by accident. We believe these data caution against oversimplifying the interpretation of isochronal annealing data. To get a more direct estimate of the effective motion energy, involving less initial assumptions, we performed isothermal anneals.

B. Isothermal Anneals

1) Isothermal anneal

For an isothermal anneal, the specimen is heated to a given temperature and the recovery measured as a function of time. For these anneals, the resistance of the specimen was measured, with a precision of a few hundredths of a per cent, 5 to 8 times during a typical 10 minute anneal. Using these measurements, the temperature was adjusted so that the positive and negative deviations from the temperature of interest were balanced. In this manner, the average temperatures from one 10 minute anneal to the next were held constant to within about 1K.

The circles in Figure 33 represent an isothermal recovery curve for specimen A annealed at 798K. The specimen was quenched from 3230K to avoid the impurity problem encountered with the isochronal anneals after lower quench temperatures. The X's are data from another 1.0 mil specimen which broke after the fourth data point was obtained. The most important point to be made about these two curves is that they are not consistent

● $T_A = 798K$ X $T_A = 800K$
● $T_Q = 3230K$ X $T_Q = 3252K$

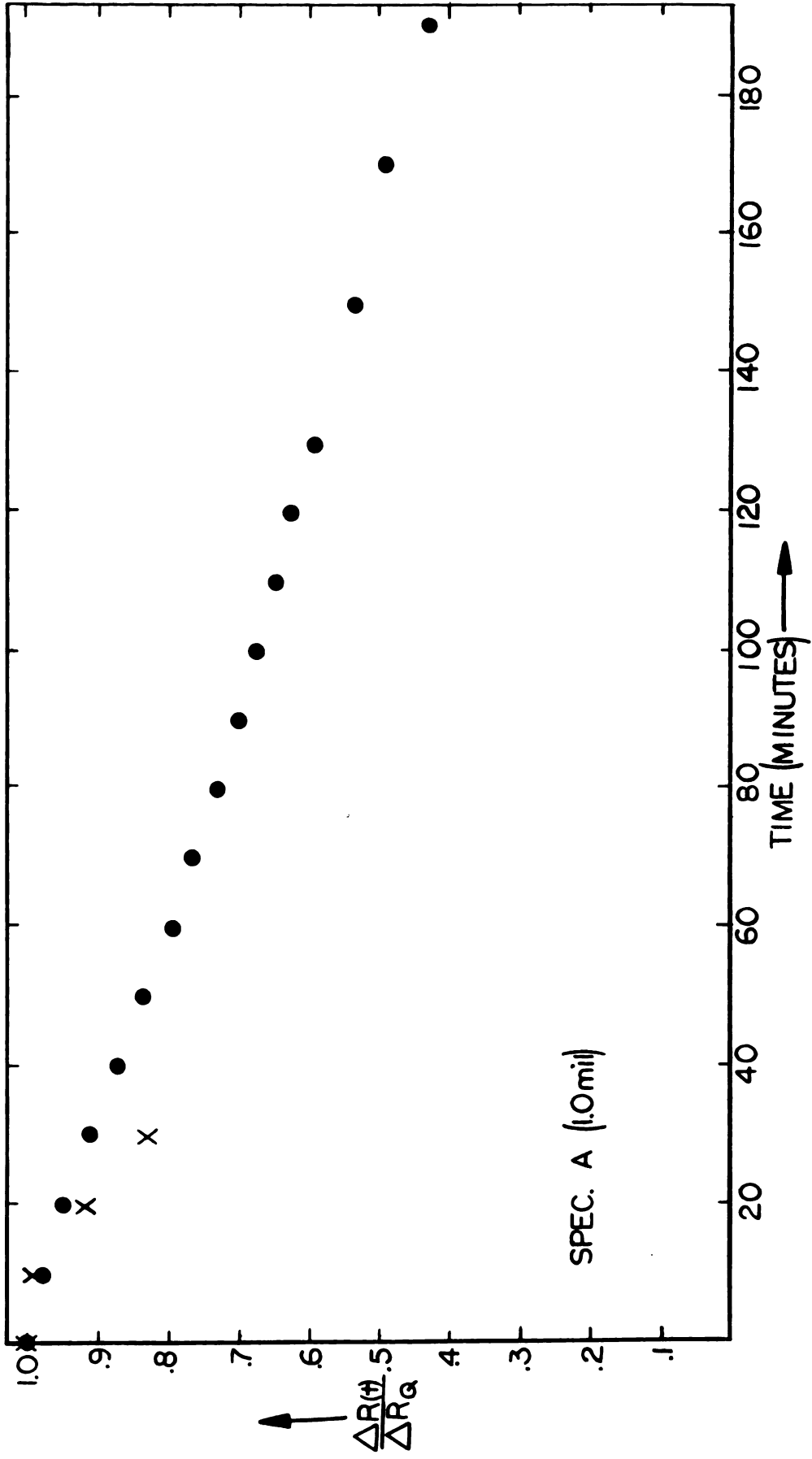


Figure 33: Isothermal Anneal

with equation (4) for any value of $\gamma \geq 0$. Equation (4) predicts that the magnitude of the slope of the annealing data in Figure 33, should always decrease with increasing time (because ρ decreases with annealing time), i.e., a curve through the data should always be concave upward. However, for short annealing times the data curve is definitely concave down, and only later does the curve go through an inflection point and become concave upward. Similar curves have been seen before, 46,47,48/ and categorized under the name, "S" shaped curves. In general, such a curve is taken as an indication that the annealing of the vacancies is a complex process, possibly involving vacancy-vacancy clustering and time varying sink densities. This "S" shaped curve was also observed in the isothermal anneals with change-of-slope measurements discussed in the next section. Other than this "S" shaped curve, the data decrease smoothly again consistent with the existence of a single major recovery stage. We had some trouble with temperature uniformity along specimen A during this anneal, hence no quantitative results were obtained from this data.

2) Isothermal anneals with change-of-slope measurements

From equation (3a), we see that if we could measure $d\rho/dt$ at two different temperatures T_1 and T_2 , under conditions where $F(\rho)$ is the same, we could obtain the energy of motion from the relation:

$$E_m^v = \frac{\ln \left[\frac{d\rho}{dt} \Big|_{t_o^1} / \frac{d\rho}{dt} \Big|_{t_o^2} \right]}{\frac{1}{k} \left(\frac{1}{T_2} - \frac{1}{T_1} \right)} \quad (9)$$

Here $\frac{d\rho}{dt} \Big|_{t_o^1}$ is the slope of the T_1 isothermal curve at a time t_o ; $\frac{d\rho}{dt} \Big|_{t_o^2}$ is the slope of the T_2 isothermal curve at the same time t_o ;

T_1 is the first annealing temperature, and T_2 is the second annealing temperature. Equation (9) forms the basis for the so-called "change-of-slope" technique introduced by Bauerle and Koehler.^{5/} In this technique, one begins an isothermal anneal at the temperature T_1 and obtains enough points to accurately determine the slope of the recovery curve $\left. \frac{d\rho}{dt} \right|_{t_0^1}$. At time t_0 , the annealing temperature is then changed to T_2 which changes the rate of annealing. Enough points are taken at the new annealing temperature T_2 to enable one to extrapolate the data back to the point t_0 , and thereby, obtain the slope $\left. \frac{d\rho}{dt} \right|_{t_0^2}$. All of the quantities on the right side of equation (9) are now known allowing the effective motion energy to be obtained.

After the recovery curve is determined sufficiently to obtain its slope at the second annealing temperature, the annealing temperature can again be changed and the above process repeated to obtain another estimate of the motion energy. This technique has the advantage that only equation (3a) is assumed to hold. The additional restrictions required to obtain equation (4) are not necessary for this analysis.

Figures 34 and 35 show the results of such measurements made on two independent 1.0 mil specimens. These specimens had 0.3 mil potential leads spot-welded on to minimize temperature non-uniformities; with these leads, no temperature variation was visible along the gauge length when the specimen was heated in vacuum until it barely glowed in a darkened room. Both of these sets of data also have the "S" shape discussed in connection with the isothermal anneals on page 87. The annealing temperatures and the effective motion energy calculated for each change-of-slope point are marked in the figures. For these experiments to give meaningful results, the data must have very little scatter, and the curve connecting

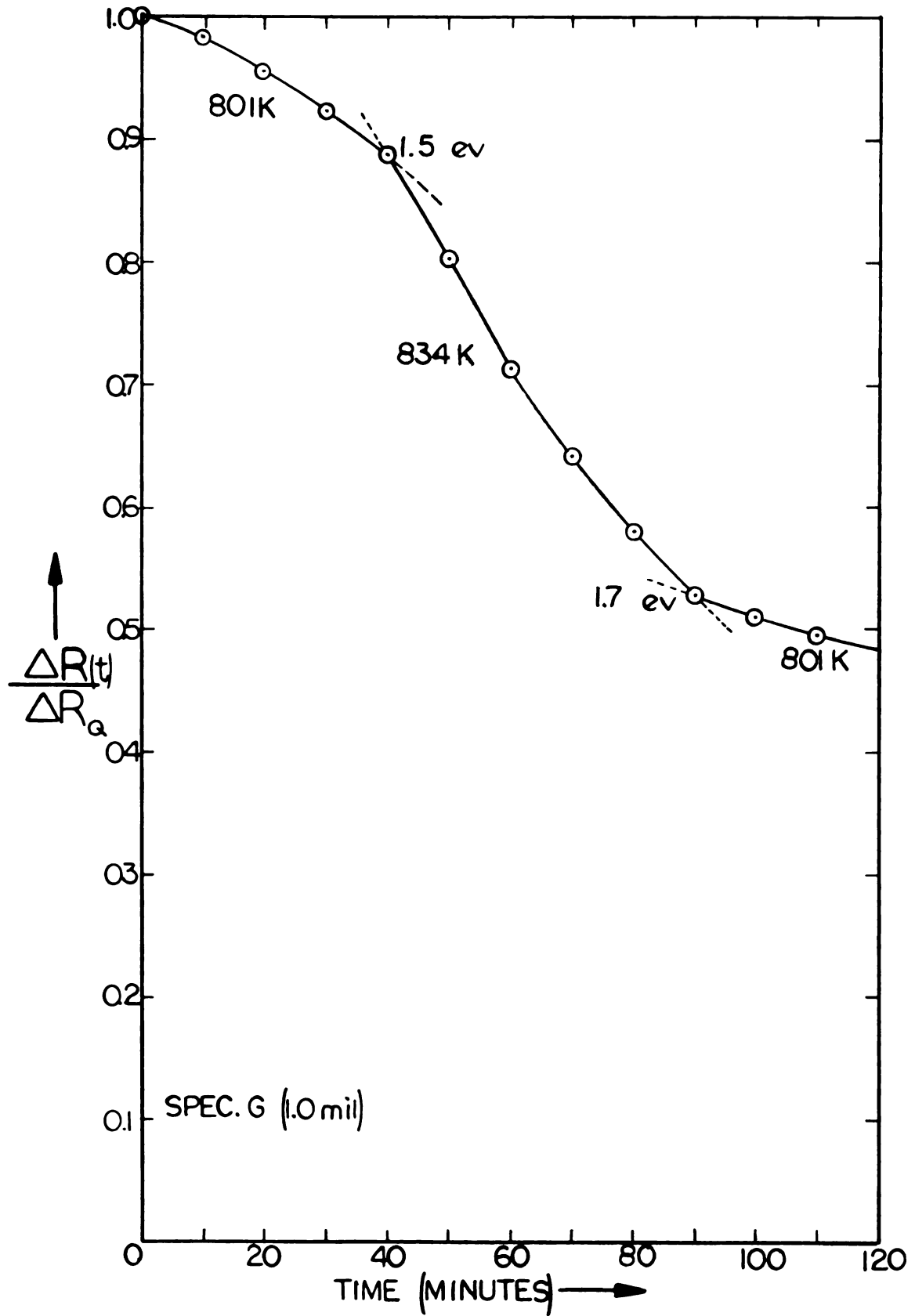


Figure 34: Isothermal Anneal with Change-of-Slope Measurements

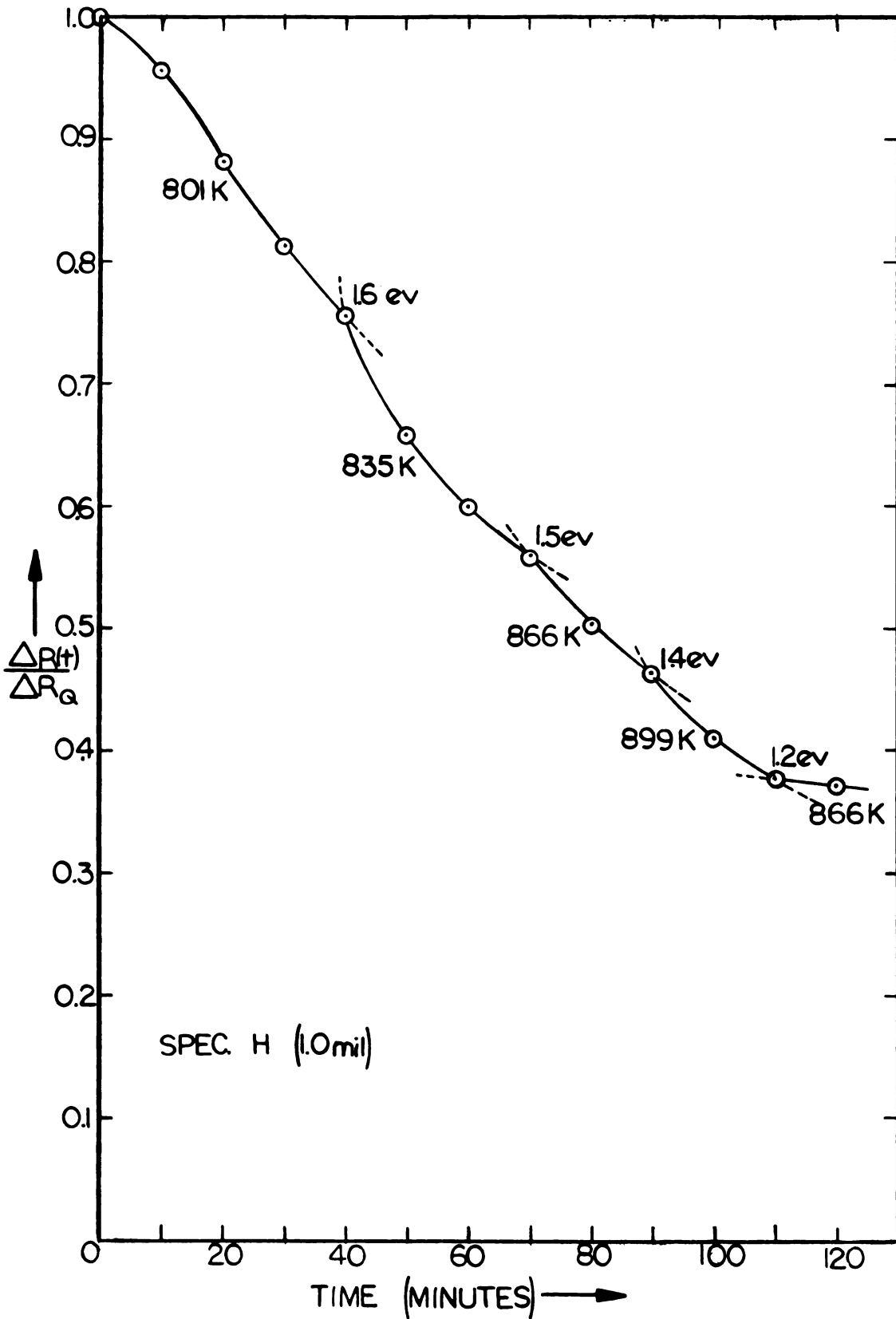


Figure 35: Isothermal Anneal with Change-of-Slope Measurements

the data points must be carefully drawn so that the slopes can be accurately determined. The curves shown in Figures 34 and 35 were drawn through the data points with the aid of French curves. A mirror placed at the point of interest was positioned to make the curve and its image appear continuous. A line was drawn along the edge of the mirror giving the normal to the curve at the change of slope point. The normal to this line then gave the slope of the curve. In this manner, the slopes could be obtained accurately to a few per cent, except possibly where there is extreme curvature.

The data give an effective motion energy of 1.5 ± 0.3 ev. It should be noted that the effective motion energies calculated here are from specimens which were quenched from very high temperatures, and only the upper two-thirds of the recovery curve was used.

The effective motion energy determined here is in good agreement with the motion energy (1.4 ± 0.2 ev) obtained above with the Flynn theory analysis. However, these effective motion energies are much lower than those obtained for Stage IV radiation damage studies (see Table 1). They are even somewhat lower than the 1.7 ev motion energies obtained for Stage III.

While the agreement on the vacancy motion energy between the Flynn analysis and change-of-slope analysis is suggestive, we do not believe that it should be taken too seriously yet. In several other metals ^{5,46/} effective motion energies measured after high temperature quenches are found to be substantially lower than the single vacancy migration energy, presumably reflecting the effects of mobile vacancy-vacancy complexes. The "S" shaped isothermal curve suggests complexities of this type are likely to be found in the annealing of tungsten. It is likely that careful annealing studies from a series of quench temperatures will be necessary to obtain a satisfactory understanding of vacancy annealing in tungsten.

VI. MOLYBDENUM

We have annealed and quenched molybdenum using the superfluid technique. A 1.5 mil specimen and a 1.1 mil specimen were annealed for six minutes at about 2350K and cooled in steps, resulting in resistance ratios of 524 and 750 respectively. Further annealing and quenching increased these ratios to 620 and 870. Surprisingly, the thinner wire had the larger resistance ratio.

Preliminary quench data for these specimens are shown in Figure 20. The 1.5 mil data is three orders of magnitude higher than the 1.1 mil data. Also the 1.5 mil data is not very temperature-dependent; suggesting that something besides vacancies are being quenched into this specimen. The data for the 1.1 mil specimen appears more likely to be due to vacancies. However, the effective formation energy is only about 1.1 ev, which is half of the value estimated by Meakin ^{24/} and Kraftmakher ^{26/}. These data are very preliminary and are reported primarily to give an indication of the difficulties which are likely to be encountered in a systematic study of vacancies quenched into molybdenum.

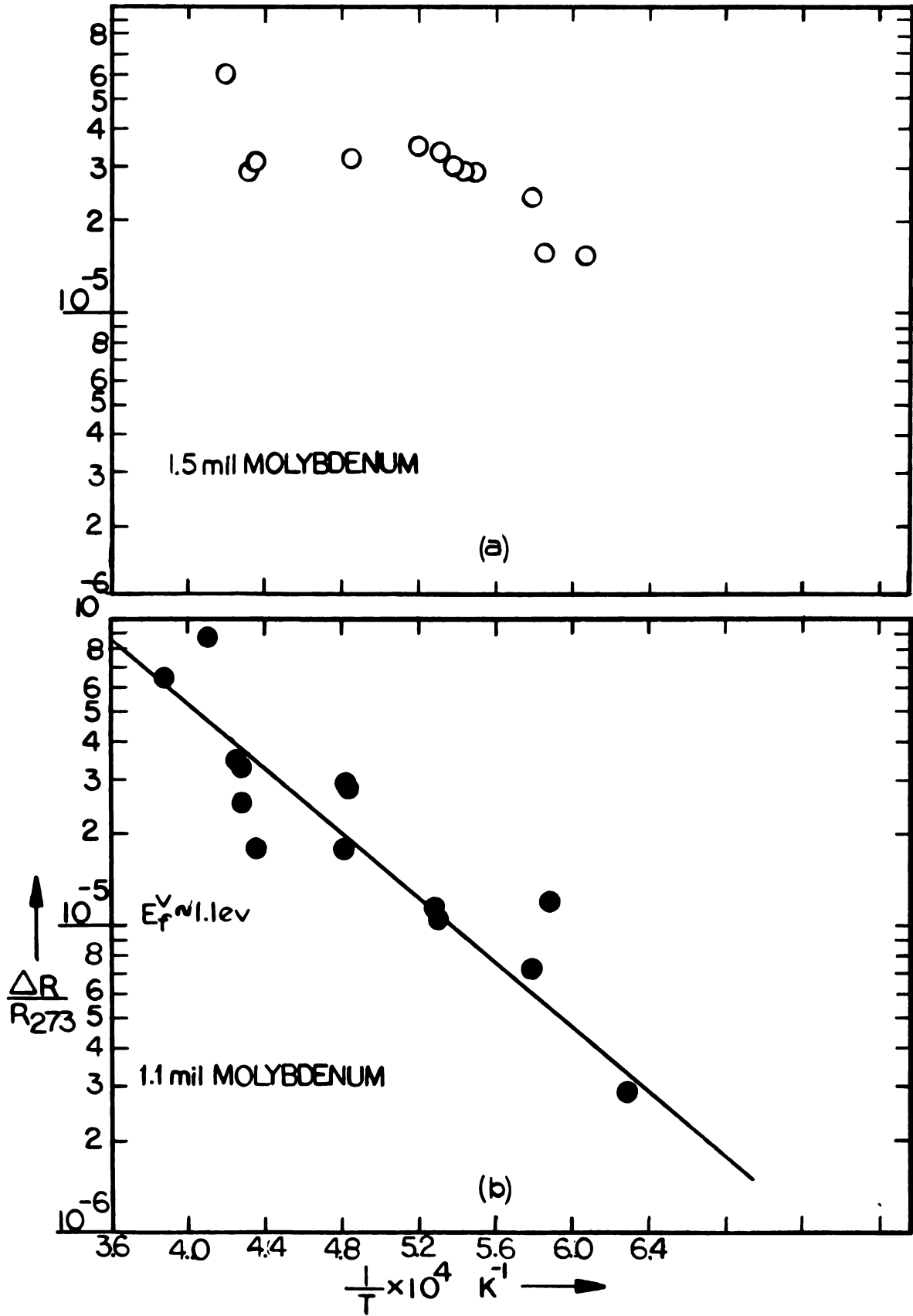


Figure 36: Preliminary Molybdenum Data

VII. SUMMARY

We have described an apparatus and technique for superfluid quenching, and have used this system to study vacancies quenched into fine tungsten wires. We have demonstrated that the quench speeds obtained are fast enough to allow studies of the dependence of quenched-in resistance on quench speed. We have found that the quenched-in resistance varies somewhat from specimen to specimen, but that the effective formation energy determined for the fast quench data is nearly the same for all specimens and equal to 3.1 ± 0.2 ev. Both the magnitude of the data and the effective formation energies are in satisfactory agreement with a similar study by Schultz. By studying how the quenched-in resistance varies with quench speed, we have shown that the equilibrium vacancy concentration is probably not being retained even with the fastest quench speeds. By extrapolating our data to infinite quench speed we can get an estimate for the vacancy formation energy, E_f^V . This extrapolation leads to the value $E_f^V = 3.5 \pm 0.2$ ev. We have also used this extrapolated data to test Flynn's theory of vacancy annealing during the quench. We find that the theory fits the infinite quench speed data, but we believe our data has slightly too much scatter to state definitively that Flynn's theory is applicable. Assuming $E_f^V = 3.5$ ev, this theory yields a value of 1.4 ± 0.2 ev for the vacancy motion energy. If the maximum value of 3.7 ev is used, a motion energy of 1.9 ± 0.6 ev results.

Isochronal and isothermal studies were made of the annealing away of the quenched-in resistance. Isochronal anneals were performed on specimens quenched from temperatures in the ranges 2800-3000K and above 3200K. There is a single major isochronal recovery stage in the temperature range 800-1000K, which is consistent with the Stage IV recovery in radiation damage studies. This single recovery stage, in which most of the quenched-in resistance anneals away, suggests that there is a single type of defect present, presumably the vacancy. The isothermal anneals were made on specimens quenched from above 3200K. These recovery curves have an "S" shape suggesting that the annealing process is complex and does not obey a simple chemical rate equation. Change-of-slope measurements yield effective motion energies of 1.5 ± 0.3 ev, in agreement with the value obtained from the Flynn analysis. Although this agreement is suggestive, it should be treated with caution. Previous experience with effective motion energies measured after high temperature quenches suggests that they are often somewhat lower than the single vacancy motion energies.

If we take our "best values" for the vacancy formation and motion energies, we obtain a value of about 5 ev for Q . This is consistent with the lower value of Q reported in recent literature. The maximum value of Q which would still be consistent with our data is $Q \cong 6$ ev. However, our data do not appear to be consistent with either $Q = 6.9$ ev, or with $E_m^V = 3.3$ ev obtained from recent radiation damage studies.

During the progress of this experiment, a number of interesting problems were uncovered which require further study. These problems will merely be listed here: 1) possible deviations from specimen to specimen

of the resistance versus temperature characteristics for tungsten; 2) resistance increase when a tungsten specimen is cycled from 4.2K to room temperature and back; 3) increase in resistance during isochronal anneals after quenches in the range of 2800 to 3000K; 4) possible complex annealing processes suggested by the "S" shaped curve; 5) superfluid bubbling phenomena; 6) problems involved in molybdenum quenching.

LIST OF REFERENCES

LIST OF REFERENCES

1. Girifalco, L. A. Atomic Migration in Crystals, Blaisdell Publishing Company, New York (1964)
2. Simmons, R. O. and R. W. Balluffi Phys. Rev. 125, 862 (1962)
3. Cotterill, R. M. J. Lattice Defects in Quenched Metals, ed. by R. M. J. Cotterill, Academic Press, New York, (1965), p97
4. Attardo, M. and J. M. Galligan Phys. Stat. Sol. 16, 449 (1966)
5. Bauerle, J. E. and J. S. Koehler Phys. Rev. 107, 1493 (1957)
6. Lazarus, D. Phys. Rev. 93, 973 (1954)
7. Schultz, H. Acta Met. 12, 761 (1964)
8. Kraftmakher, Ya. A. Soviet Physics--Solid State (USA) 4, 1662 (1963)
9. Thompson, M. W. Phil. Mag. 5, 278 (1960)
10. Vasil'ev, V. P. and S. G. Chernomorchenko Zav. Lab. 22, 688 (1956)
11. Kinchin, G. H. and M. W. Thompson J. Nucl. Energy 6, 275 (1958)
12. Koo, R. C. Reactive Metals, vol. 2, ed. by W. R. Clough, Interscience Publishers, Inc., New York (1959), pp. 265-274
13. Schultz, H. Z. Naturforschg. 14a, 361 (1959)
14. Schnitzel, R. J. Appl. Phys. 30, 2011 (1959)
15. Neimark, L. A. and R. A. Swalin Transactions, Metallurgical Soc., Am. Inst. Mining, Metallurgical, Petroleum Engrs., 218 (1960), pp 82-87
16. Danneberg, W. Metall. 15, 977 (1961)
17. Schultz, H. Acta Met. 12, 649 (1964)
18. Moteff, J. and J. P. Smith Flow and Fracture of Metals and Alloys in Nuclear Environments, Special Technical Publication #380 American Society for Testing and Materials, 171 (1965)

19. Andelin, R. L., J. D. Knight, and M. Kahn *Trans. AIME (USA)* 233, 19 (1965)
20. Jeannotte, D. and J. M. Galligan *Phys. Rev. Letters* 19, 232 (1967)
21. Keys, L. K., J. P. Smith, and J. Moteff *Phys. Rev.* 176, 851 (1968)
22. Flynn, C. P. *Phys. Rev.* 171, 682 (1968)
23. Gregory, D. P. *Acta Met.* 11, 623 (1963)
24. Meakin, J. D., A. Lawley, and R. C. Koo *Appl. Phys. Letters (USA)* 5, 133 (1964)
25. Nihoul, J. *Phys. Status Solidi.* 2, 308 (1962)
26. Kraftmakher, Ya. A. *Soviet Physics--Solid State (USA)* 6, 396 (1964)
27. Cotterill, R. M. J., ed. Lattice Defects in Quenched Metals, Academic Press, New York (1965)
28. International Conference on Vacancies and Interstitials in Metals, Sept. 23-28, 1968, Kernforschungsanlage Julich, Germany
29. Rinderer, L. and H. Schultz *Phys. Letters (Ger.)* 8, 14 (1963)
30. Martin, D. G. *Acta Met.* 5, 371 (1957)
31. Borisov, E. V., P. L. Gruzin, L. V. Paulinov, and G. B. Fedorov
Collection: Metallurgy and Metallography of Pure Metals (in Russian) (Izd. MIFI, Moscow, 1959), # 1
32. Peiffer, H. R. *J. Appl. Phys.* 29, 1581 (1958)
33. Danneberg, W. Z. *Naturforsch.* 16a, 854 (1961)
34. Peacock, D. E. *Phil. Mag. (GB)* 8, 563 (1963)
35. Askill, A. and D. H. Tomlin Diffusion in Body-Centered-Cubic Metals
American Society for Metals, Metals Park, Ohio (1964), p 247
36. Temperature, Its Measurement and Control in Science and Industry,
Reinhold Publ. Co. , New York, (1941), p. 1318
37. Jones, H. A. and I. Langmuir *Gen. Elec. Rev.* 30, 310 (1927)
38. Davis, G. L. *Nature (GB)* 196, 565 (1962)
39. Kuhlmann, H. H. and H. Schultz *Acta Met.* 14, 798 (1966)

40. Goldschmidt, H. J. and J. A. Brand *J. Less-Common Metals* 5, 181 (1963)
41. Kauffman, J. W. and M. Meshii *Lattice Defects in Quenched Metals*, ed. by R. M. J. Cotterill, Academic Press, New York (1965), p 77
42. Jackson, J. J. *Lattice Defects in Quenched Metals*, ed. by R. M. J. Cotterill, Academic Press, New York (1965), p 467
43. Balluffi, R. W., R. W. Siegel, K. H. Lie, D. N. Seidman *International Conference on Vacancies and Interstitials in Metals*, Sept. 23-28, 1968, Kernforschungsanlage Julich, Ger.
44. Flynn, C. P., J. Bass, and D. Lazarus *Phil. Mag.* 11, 521 (1965)
45. Neely, H. H., D. W. Keefer, and A. Sosin *Phys. Stat. Sol.* 28, 675 (1968)
46. Ytterhus, J. A., R. W. Siegel and R. W. Balluffi *Lattice Defects in Quenched Metals*, ed. by R. M. J. Cotterill, Academic Press, New York, (1965), p 683
47. Federighi, T. *Lattice Defects in Quenched Metals*, ed. by R. M. J. Cotterill, Academic Press, New York (1965), p 217
48. de Jong, M. and J. S. Koehler *Phys. Rev.* 129, 40 (1963)
49. Malmstadt, H. V. and C. G. Enke *Electronics for Scientists*, W. A. Benjamin, Inc., New York (1963), pp. 341-383

APPENDICES

APPENDIX A

Significance of the Superfluid

The fact that superfluid is not essential for this experiment was discovered accidentally during a test of the "radiation shield" described in Section IV E. The specimen was at a high temperature (about 3000K) in the superfluid; after 2 to 3 minutes the liquid around the specimen began to bubble indicating that the liquid near the specimen was no longer superfluid even though the pressure was still in the 1-5 Torr range. Further tests indicate that bubbles form around the specimen and float to the top until the specimen is about 3/4 inch below the surface. If the specimen is lowered further, bubbles seem to form along the specimen, but do not leave it to rise to the surface. If the specimen is lowered still further (below about 1-1/2 inch), these bubbles form only at the ends of the specimen. They also appear to be smaller, and again do not float away from the specimen. If the specimen is placed slightly below the depth where the bubbles rise to the surface, there seems to be "pulsation", the bubbles rise to the surface for a while, then stop and start again. The period of these "pulsations" is of the order of a second.

During all of these tests, as nearly as one can tell by eye, neither the average temperature nor the temperature uniformity of the specimen changed significantly. This fact was verified by direct readout of the spec-

imen resistance on a digital voltmeter. This is direct proof that bubble formation around the specimen does not burn it out, or ruin the experiment. This implies that the superfluid is not necessary.

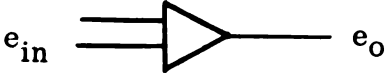
We believe that the superfluid around the specimen turns normal because the radiation shield restricts the flow of the superfluid. This causes the superfluid to reach its critical velocity and turn normal when it passes through the holes in the radiation shield. More study of this phenomena is necessary before it can be adequately explained.

APPENDIX B

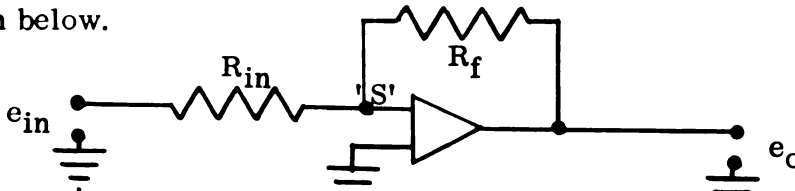
Operational Amplifiers

To assist the reader in understanding the AC circuits, a brief description of operational amplifiers is given. The symbol for an operational amplifier

is:



The principal characteristics of a typical operational amplifier are high input impedance, high gain (100,000), and good frequency response. The operational amplifier alone is no better than a conventional amplifier. The addition of the negative-feedback path (control loop) makes the amplifier circuit stable and suitable for accurate control. A simple operational feedback circuit is shown below.



The feedback impedance R_f connects the output of the amplifier to the input.

The amplifier's very high gain and phase reversal makes point 'S' (the summing point) a "virtual ground," i.e., it is ideally at ground potential but not connected to the ground. Hence the input current i_{in} is just e_{in}/R_{in} .

Since the voltage at 'S' is zero we see that the output voltage is just $-R_f i_{in}$.

Substituting for i_{in} from above, gives the important result, $e_o = -(R_f/R_{in}) e_{in}$.

That is, the output voltage is directly proportional to the input voltage with the gain given by R_f/R_{in} . Since these impedances can be made quite stable,

the gain of the operational amplifier can be made very constant. This is important in the AC amplifier system described in Section III C 2).

For a constant current source, the load is put in the place of R_f . The output voltage will then always adjust itself so that the current through the load is e_{in}/R_{in} as described above. This will remain true so long as the operational amplifier is not overloaded.

MICHIGAN STATE UNIVERSITY LIBRARIES



3 1293 03061 8726